



**NIST** United States Department of Commerce  
National Institute of Standards and Technology

***NISTIR 3968***

**Report No. 23**

**RESIDUAL STRESS DETECTION IN  
RAILROAD WHEELS:  
AN ULTRASONIC SYSTEM USING EMATS**

---

---

Raymond E. Schramm  
Alfred V. Clark, Jr.  
Dragan V. Mitraković  
Stephen R. Schaps  
Todd J. McGuire

QC

100

.U56

3968

1991

C.2



**NISTIR 3968**

**Report No. 23**

**RESIDUAL STRESS DETECTION IN  
RAILROAD WHEELS:  
AN ULTRASONIC SYSTEM USING EMATS**

---

---

Raymond E. Schramm  
Alfred V. Clark, Jr.  
Dragan V. Mitraković\*  
Stephen R. Schaps  
Todd J. McGuire

Materials Reliability Division  
Materials Science and Engineering Laboratory  
National Institute of Standards and Technology  
Boulder, Colorado 80303-3328

\*NIST Guest Researcher, on leave from the University of Belgrade

May 1991

Prepared for  
U.S. Department of Transportation  
Federal Railroad Administration  
Office of Research and Development  
Washington, DC 20590



---

U.S. DEPARTMENT OF COMMERCE, Robert A. Mosbacher, Secretary  
NATIONAL INSTITUTE OF STANDARDS AND TECHNOLOGY, John W. Lyons, Director



## CONTENTS

	Page
ABSTRACT .....	1
INTRODUCTION .....	2
CONTRACT HISTORY .....	3
STRESS MEASUREMENT METHODS	
Saw Cutting .....	4
X-Ray Diffraction .....	4
Neutron Diffraction .....	4
Hole Drilling .....	5
Visual Appearance .....	5
Acoustic .....	5
ACOUSTIC BIREFRINGENCE AND STRESS .....	6
EMAT OPERATION .....	7
Principles .....	7
Configuration .....	8
OPERATIONAL PRINCIPLES .....	12
Transducer Package and Fixture .....	12
EMAT Electronics .....	14
Digital Gate .....	17
Interval Timer .....	18
SYSTEM ASSEMBLY AND USAGE	
Wheel Mount System .....	19
Connections and Cables .....	19
Data Collection .....	20
EXPERIMENTAL RESULTS	
EMAT/PZT Comparison .....	21
Stress Sensitivity .....	22
Saw-Cut Comparison .....	24
Texture Measurement .....	24
ELECTRONIC CIRCUITS .....	25
CHECKLIST .....	39
TROUBLE SHOOTING .....	39
FUTURE CONSIDERATIONS .....	40
ACKNOWLEDGMENTS .....	40
REFERENCES .....	41



RESIDUAL STRESS DETECTION IN RAILROAD WHEELS:  
AN ULTRASONIC SYSTEM USING EMATS

Raymond E. Schramm, Alfred V. Clark, Jr.,  
Dragan V. Mitrakovic,\* Stephen R. Schaps, and Todd J. McGuire

Materials Reliability Division  
Materials Science and Engineering Laboratory  
National Institute of Standards and Technology  
Boulder, Colorado 80303-3328

\* NIST Guest Researcher, on leave from the University of Belgrade

This is report number 23 in a series covering research performed by the National Institute of Standards and Technology for the Federal Railroad Administration. This report covers a project by the Materials Reliability Division (formerly the Fracture and Deformation Division) to develop and build a system to detect and measure residual stress in the rims of railroad wheels.

Acoustic birefringence is the underlying principle of operation. This is a measure of the relative difference in the propagation times of two shear waves polarized in radial and circumferential directions. Measurements employ an EMAT (electromagnetic-acoustic transducer) as an ultrasonic probe. This type of transducer requires little or no surface preparation and no acoustic couplant. The system operates in a pulse-echo mode. A short burst of shear horizontal waves travels through the rim thickness. The rotation of the EMAT determines the orientation of the polarization vector, radial or circumferential. Precise timing of echoes in both directions reveals the degree of birefringence. Changes are due to both stress state and metallurgical texture. Initial tests indicate it may be possible to separate these two.

This report documents the design, construction, and testing of the system. It is also to serve as an operational guide for the equipment being delivered to the FRA.

Key words: birefringence; EMAT; nondestructive testing; railroad wheel; residual stress; ultrasonic.

## INTRODUCTION

In this country, most railroad operations now deal with the transportation of freight in its many forms. Modern needs place ever greater demands on the elaborate rail network that began developing early last century. Just one of the important elements in this complex system is the integrity of the many wheels that bear the loads. As massive as the cast-steel wheels used in the U.S. are, they might not seem to be a problem. Accident statistics, however, indicate otherwise. According to the Accident/Incident Bulletin of the FRA Office of Safety, broken wheels caused 134 accidents in the four year period of 1985-1988, resulting in losses totaling \$27.5M. Besides the direct and indirect cost of such problems, there is the threat to human life and health due to the accidents themselves or the potential environmental impact from the release of dangerous materials. Disruption to commerce at many levels is almost inevitable.

During their lifetime, wheels see a wide variety of sometimes extreme conditions. Among these are large static and dynamic mechanical loads, large-scale frictional wear, high temperatures from braking operations, environmental extremes, and exposure to potentially corrosive materials. All these factors operate to initiate tread cracks or aggravate any existing faults. Depending on the stress conditions (applied and residual), crack growth can be very slow and gradual or rapid, even explosive. The relative rarity of failures under all these extreme conditions speaks well for the progress made in wheel design and manufacture.

Wheel improvements will continue, but it will not be possible to eliminate completely the tensile stresses that drive a crack to failure. For economic, environmental, and safety reasons, replacement before failure is the preferred approach. Because of the costs and uncertainties involved, retirement for cause is favored, whenever possible, over replacement at predetermined intervals. Effective and efficient nondestructive evaluation makes it possible to evaluate fitness for service. For railroad wheels, as in most other applications, the first NDE test is visual examination by a skilled inspector. In practice, however, this simple approach has severe limitations. The stress state itself is not directly observable. The ideal test method would be simple, reliable, unintrusive, inexpensive, and operator independent. No available techniques fulfill all these conditions perfectly, but ultrasonic testing offers a possible major step in this direction.

The ultrasonic system examined here follows upon prior efforts at NIST and elsewhere, and upon the experience and expertise with electromagnetic-acoustic transducers in this laboratory. After laboratory testing and development, we built a prototype for delivery to the FRA. This will receive extensive field testing and exposure to potential users. The desired goal is to develop an instrument of value to the railroad industry that private industry would license for commercial production.

The intention here is to develop an instrument for use in a railcar shop during maintenance operations. Subsequent developments may allow use at trackside should this prove desirable.

## CONTRACT HISTORY

As the Fracture and Deformation Division of the National Bureau of Standards, we first received a Federal Railroad Administration research contract to develop nondestructive evaluation (NDE) procedures for railroad wheels in September 1985. During the period of this work, we have been renamed the Materials Reliability Division of the National Institute of Standards and Technology. Our contract monitors have been M. Clifford Gannett, Claire Orth, and Donald E. Gray. The current contract is Reimbursable Agreement No. DTFR53-89-X-00018 with an effective date of 4/21/89.

Over the past few years, we presented the results of the work done under this sponsorship at two meetings:

1. Review of Progress in Quantitative Nondestructive Evaluation, La Jolla, California, August 1986.
2. 1987 IEEE Ultrasonics Symposium, Denver, Colorado, October 1987.

There have been four publications on this part of the work:

1. "Ultrasonic Characterization of Residual Stress and Texture in Cast Steel Railroad Wheels," A. V. Clark, H. Fukuoka, D. V. Mitrakovic, and J. C. Moulder in Review of Progress in Quantitative Nondestructive Evaluation, Vol. 6B, D. O. Thompson and D. E. Chimenti, eds., Plenum Press, New York (1987), 1567-1575.
2. "Characterization of Residual Stress and Texture in Cast Steel Railroad Wheels," A. V. Clark, Jr., H. Fukuoka, D. V. Mitrakovic and J. C. Moulder, Ultrasonics 24, 281-288 (1986).
3. "Ultrasonic Characterization of Residual Stress and Flaws in Cast Steel Railroad Wheels," A. V. Clark, R. E. Schramm, H. Fukuoka, and D. V. Mitrakovic in Proceedings: IEEE 1987 Ultrasonics Symposium, B. R. McAvoy, ed., Institute of Electrical and Electronic Engineers, New York (1988), 1079-1082.
4. "Acoustoelastic Measurements Pertaining to the Nondestructive Characterization of Residual Stress in a Heat-Treated Steel Railroad Wheel," A. V. Clark, H. Fukuoka, D. V. Mitrakovic, and J. C. Moulder, Materials Evaluation 47, 835-841 (1989).

Most of this material was collected together and published as:

Report No. 18: Ultrasonic Railroad Wheel Inspection Using EMATs, Raymond E. Schramm and A. Van Clark, Jr., NISTIR 88-3906, Dec. 1988.

Other work done under this contract focused on the detection of cracks in the tread of railroad wheels. The approach has been to use an in-rail EMAT to generate Rayleigh waves and listen for flaw echoes. Operation will be roll-by and fully automatic. The results of this parallel study are in a prior NISTIR 91-3967:

Report No. 22: Tread Crack Detection in Railroad Wheels: An Ultrasonic System Using EMATs.

## STRESS MEASUREMENT METHODS

Following are a few observations on some of the usual techniques.

### Saw Cutting

While obviously not usable for in-service inspection, destructive methods do usually provide definitive measurements and can provide verification of nondestructive procedures. In the case of railroad wheels, one approach is to make saw cuts along the radius. The presence of compressive or tensile stresses will cause the wheel to close on the blade or open further. Quantitative measurements of stress and its distribution are possible by careful instrumentation with strain gages. Because of the complex shape of a wheel, it is generally necessary to enter these data into some model (such as finite element) for considerable calculations to reveal the stress state.

### X-Ray Diffraction

The strains caused by residual stresses are evident even at the level of interplanar spacing within the crystal lattice. The exact angular position of X-ray powder diffraction lines is a very sensitive indicator of such changes. Commercial devices designed for this specific task are on the market. The main limitations of this approach fall into two categories:

1. All measurements must be referred to a stress-free specimen. At the interatomic level, such a state is difficult to achieve and also tends to be very dependent on exact chemistry and metallurgy.
2. X-rays penetrate only several atomic layers deep. The resulting calculations reflect the status at the immediate surface, while the stress distribution likely has a very sharp gradient there. The stresses internal to thick materials can only be inferred.

### Neutron Diffraction

Another way of measuring the interatomic strains is by looking at the diffraction of neutrons caused by the periodicity of the nuclear magnetic moments. Because of the great penetrating power of neutrons, it is possible to obtain the stresses deep within very large specimens. Unfortunately, the usual source of radiation is a nuclear reactor. The measurement instrumentation also is usually bulky and complex. While this is a valuable research tool, it rarely sees service in an industrial setting.

## Hole Drilling

A mature technique that is "mostly" nondestructive is the measurement of strain relief while drilling a very precise, shallow hole into the surface of the specimen. Special strain gage rosettes and milling fixtures specially designed for this purpose are commercially available. Assuming that the damage from the small hole is acceptable, there are two problems:

1. The procedure is very time consuming and requires considerable skill and experience.
2. Measurements represent the stress state within the top few millimeters of the specimen. Again, conditions deep inside must be inferred.

## Visual Appearance

If a stress state is due to transient high-temperature conditions, there may be evidence in the form of surface discolorations from oxidation reactions. In fact, the Federal Railroad Administration, DOT, Code of Federal Regulations 49 CFR states:

‡215.103 Defective wheel

A railroad may not place or continue in service a car if -

...

(h) A wheel on the car shows signs of having been overheated as evidenced by a reddish brown discoloration, to a substantially equal extent on both the front and the back face of the rim, that extends on either face more than four inches into the plate area measured from the inner edge of the front or back face of the rim ...

The obvious problem here is the need for a color-calibrated eye and excellent lighting conditions. In addition, destructive tests done by the Transportation Test Center (TTC) on wheels condemned by this rule showed that approximately half (more for Class C) of them contained compressive hoop stresses and were still safe for service.

## Acoustic

The theoretical effects of stress on the propagation of sound and a considerable body of experimental work have been known for some time, much of it done in this laboratory [1,2]. While most of this has involved the relations between stress, polarization direction, and velocity, the magneto-acoustic effect has been under study by the Association of American Railroads (AAR) [3]. A commercial device with special reference to railroad applications is now available [4].

Acoustic methods have two possible problem areas:

1. Very high precision in signal timing is necessary to determine velocity with sufficient precision.
2. It may be necessary to have a reference material representing the metallurgical texture of the unstressed specimen.

With the expectation of overcoming these difficulties, we have chosen to pursue the application of EMATs to the measurement of acoustic birefringence for the calculation of residual stress.

### ACOUSTIC BIREFRINGENCE AND STRESS

Birefringence (or double refraction) is the variation of the propagation velocity of a wave with the direction of the polarization vector. This property is probably most familiar as an optical phenomenon in some natural crystals, such as calcite. Some polymers exhibit a photoelastic effect; i.e., their birefringence is a function of mechanical stress. Such materials are available commercially, and they permit a visual representation of the development of an applied surface stress field.

Acoustic waves in anisotropic materials exhibit birefringence. There are two principal causes for this: stress fields and metallurgical texture or preferred orientation of grains. While there are several ways to probe this anisotropy [1,2], Fig. 1 illustrates the approach pursued in this

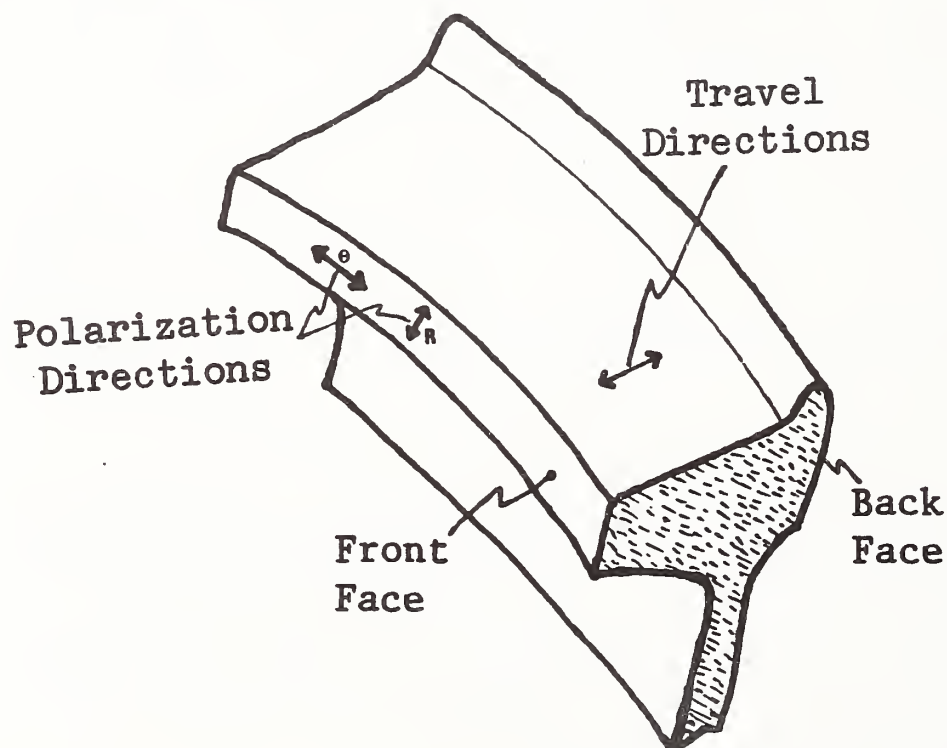


Figure 1. Schematic of a section of wheel rim indicating the travel and polarization directions of the ultrasonic pulse.

work. We place a transducer on the front face of the wheel rim and launch an ultrasonic pulse through the thickness of the rim. This pulse will reflect back toward the transducer from the back face, and its transit time is indicative of the velocity. The ultrasound is a horizontally polarized shear wave. There are two timing measurements necessary, with the polarization vector oriented along the radial (R) direction and tangential to the wheel circumference ( $\theta$ ). To achieve this, the transducer remains in the same location and simply rotates  $90^\circ$ . The distance traveled by the two pulses is exactly the same, so the experimental parameters are their arrival times. We define the birefringence as the fractional change in the velocity of the two polarizations:

$$B = (V_\theta - V_R) / (V_\theta + V_R)/2 = (t_R - t_\theta) / (t_R + t_\theta)/2. \quad (1)$$

B is the birefringence; V is the velocity, and t is the transit time of waves polarized in the R and  $\theta$  directions.

The functional relationship between birefringence and stress is:

$$B = B_0 + C_A(\sigma_\theta - \sigma_R).$$

$B_0$  is the birefringence due to the metallurgical texture.  $C_A$  is the stress acoustic constant. The  $\sigma$ 's are the stresses in the principal directions.

The value of  $C_A$  for shear waves is small [6], about  $-7.0 \times 10^{-6} \text{ (MPa)}^{-1}$  or  $-4.8 \times 10^{-5} \text{ (ksi)}^{-1}$  for steel wheels. Effectively, this means that the timing measurements must be very accurate (typically a few parts in  $10^5$ , or  $<10 \text{ ns}$  in a  $100 \mu\text{s}$  interval).  $B_0$  is usually a significant or major portion of the total birefringence, B. If we know  $B_0$  (e.g., from a measurement on an unstressed specimen), the stress difference is then

$$\sigma_\theta - \sigma_R = (B - B_0) / C_A. \quad (2)$$

Usually,  $\sigma_R$  is negligible.

## EMAT OPERATION

EMATs (electromagnetic-acoustic transducers) are devices that generate and detect sound energy directly in an electrically conductive specimen. A major advantage of these devices is that they do not require the acoustic couplants usually associated with piezoelectric transducers. This simplifies operation and eliminates echoes and mode conversions that might occur at the interfaces the signal would otherwise have to traverse. Furthermore, they can operate effectively on rough and pitted surfaces.

### Principles

To indicate basic EMAT operation, Fig. 2 shows a primitive element composed of a wire conductor carrying a dynamic current  $I_\omega$  and a source of strong

magnetic field  $H_0$ . The current  $I_\omega$  induces dynamic eddy currents  $J_\omega$  in the metal conductor surface.  $H_0$  causes the deflection of the moving electrons in a direction defined by  $J_\omega \times H_0$ . The resultant Lorentz body forces,  $T$ , generate ultrasonic signals that propagate radially into the specimen.

The polarization and propagation direction of a signal from an EMAT are the result of the orientation of the electric and magnetic fields and the arrangement of the primitive elements. For the examination of the wheel rim, we want a shear horizontal (SH) wave (polarization vector in the plane of the specimen surface) that travels normal to the surface. To generate this ultrasonic signal, we used a planar coil (Fig. 3). This configuration involves several design considerations generated here and elsewhere [5]:

1. Because the two coils are counter-wound and connected as shown in Fig. 3, ambient or stray magnetic fields will generate electrical signals of opposite sign in the two halves. This gives noise cancellation within the transducer.
2. To prevent the generation of confusing eddy currents within the specimen, there is an electromagnetic window to define the desired area of the coil. Here, the window (unshaded area in Fig. 3) is a 1 cm square etched in copper cladding on a Kapton substrate (0.03 mm of Cu on 0.15 mm of Kapton). The rf current direction in all the exposed wires is in the same direction.
3. The coils are in the shape of an elongated spiral so that all the wires within the window are parallel. This geometry and the window combine to insure that the eddy currents generated at the specimen surface are well defined.
4. This balanced-coil geometry places the window at the center. A large, single coil can generate the same acoustic signal, but the window must then be offset to one side. This may cause some difficulty in the physical construction of the transducer.

The ultrasonic pulses resulting from this careful design can be understood and controlled. This coil is currently laid out by hand, but automatic production is possible for large quantities.

While EMATs cannot operate efficiently at large liftoffs (distance to the workpiece), they can generally tolerate a separation on the order of millimeters, and this simplifies field applications. Another EMAT advantage is its high degree of selectivity, an ability to reject most signals with an undesired polarization. This means a simpler echo pattern and less confusion in data interpretation.

### Configuration

In the present design (Fig. 3), there are 35 turns of AWG 36 enameled wire in each half of the coil. The turns are tightly packed as they are wound into the mastic on a thick polymer tape. The aim is to get as many turns as possible into the available space. The DC resistance of the connected pair of coils is approximately 5.0  $\Omega$ .

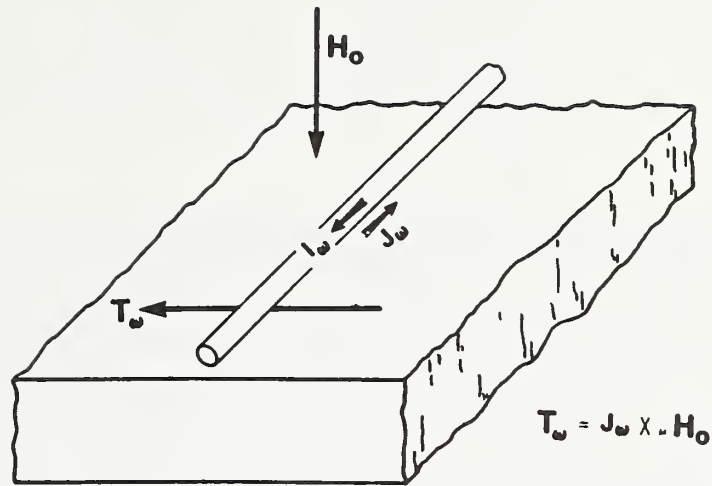


Figure 2. Primitive EMAT element.

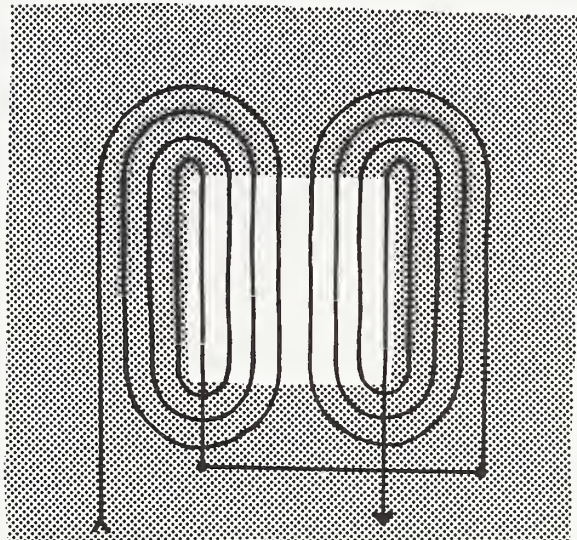


Figure 3. Schematic of the EMAT coil used to generate and receive shear horizontal (SH) waves. The 35 turns of AWG 36 enameled wire in each of the two coils are tightly packed as they are wound into the mastic on a thick polymer tape. This shows the manner of connecting the two counter-wound halves. The shaded area is a thin copper shield with a 1 cm square window over the active section.

The permanent magnet supplying the field is a 52 mm × 26 mm × 31 mm block of Nd-Fe-B with a nominal energy product of 0.28 MJ/m<sup>3</sup> (35 MG·Oe). The field direction is along the 31 mm dimension and must be normal to the test surface. To confine and concentrate the field into the area of interest, there is a tapered pole tip made from a bar of cold-rolled, mild steel (Fig. 4).

A commercial aluminum case contains the magnetic pieces and the electrical connections (Fig. 5). In this instance, the case is 105 mm high with a specimen contact area of 70 mm × 42 mm. An opening machined to fit the tip of the pole piece allows closer magnetic coupling to the workpiece and mechanically fixes the tip location. The set screws hold the magnet securely in place. A thin layer of copper tape over the pole tip shields it from the electromagnetic field of the coil, and prevents sound generation in the pole piece and the confusion this extraneous signal would generate. The next layer is the coils on their polymer tape backing. The unshaded portion in Fig. 3 must lie over the pole tip. The outer wrap in Fig. 5 is copper-clad Kapton; the etched window must also line up with the pole tip. The copper on the wrap is on the inside so the Kapton serves as a wear plate.

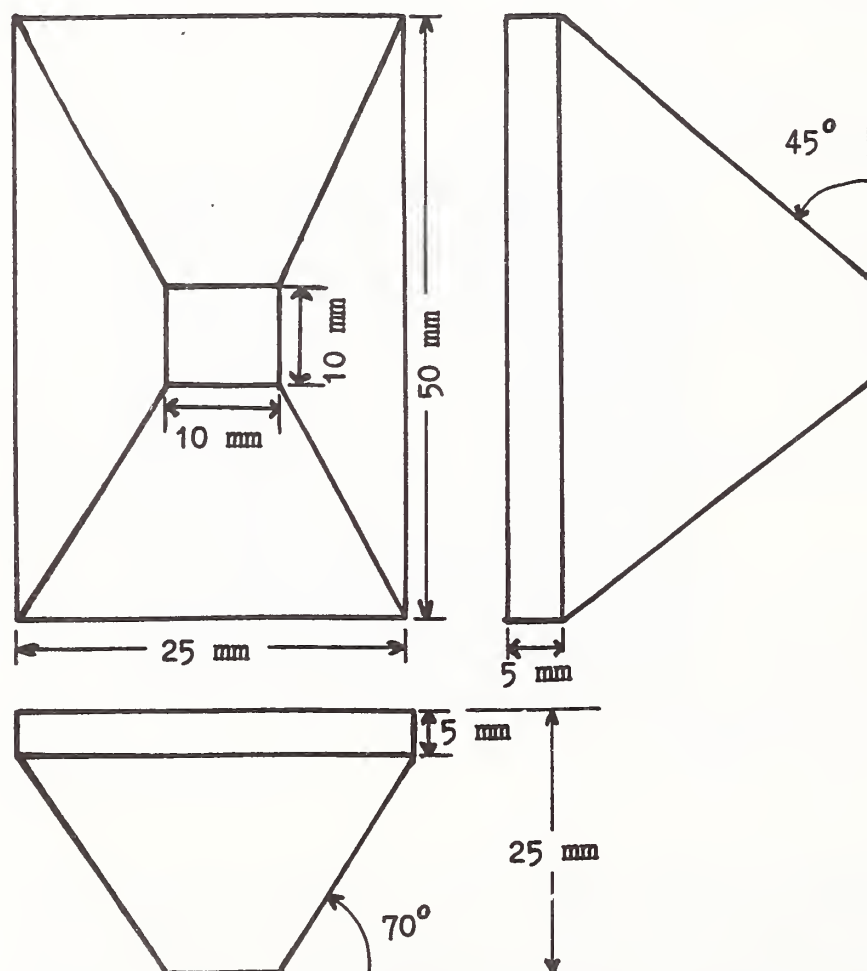


Figure 4. Configuration and dimensions of the cold-rolled, mild steel pole tip. This confines and concentrates the field from a Nd-Fe-B magnet. See Fig. 5.

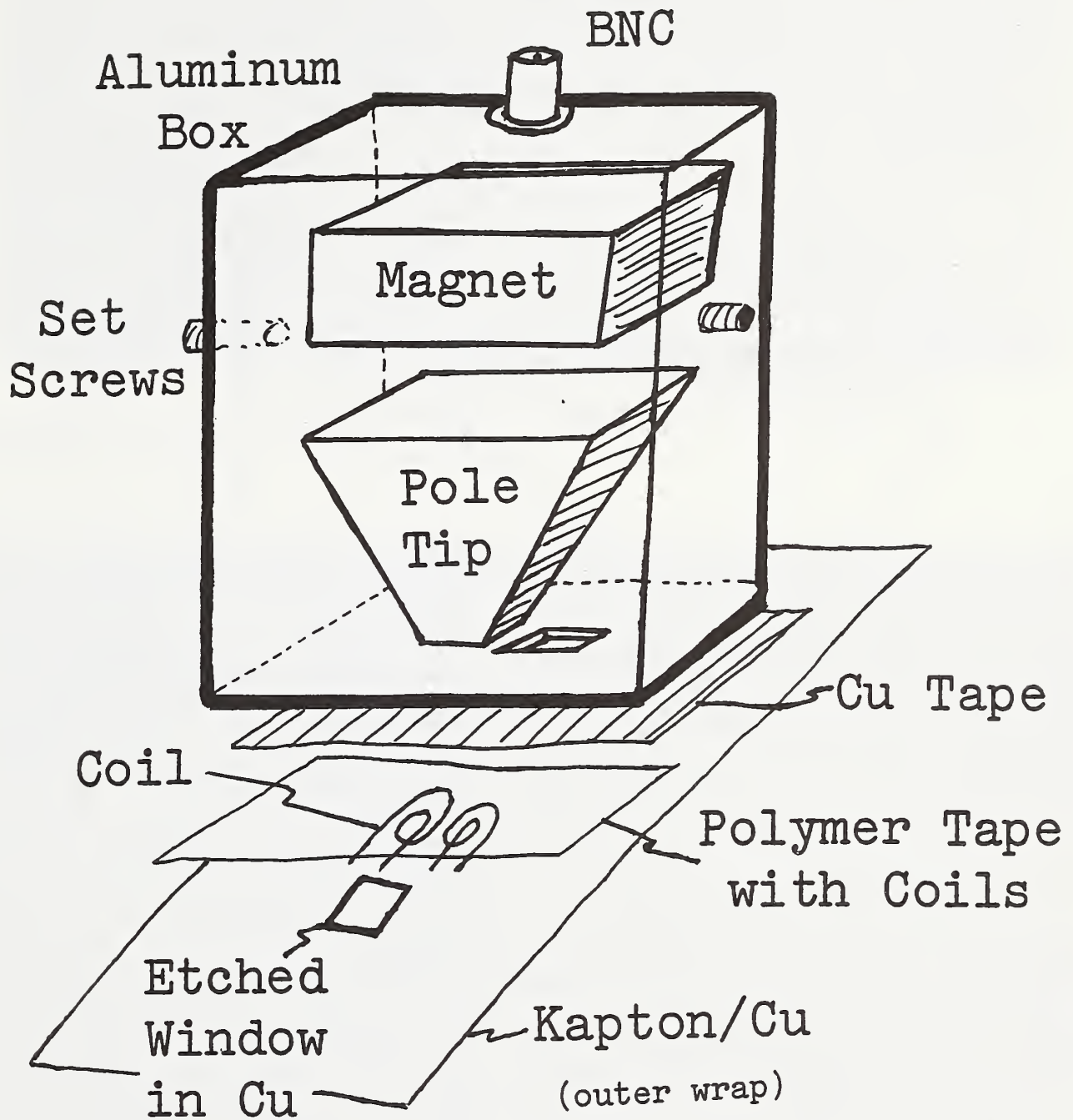


Figure 5. Schematic assembly of the EMAT. The pole tip, coils, and etched window must be carefully aligned. On the outer wrap, the copper cladding is inside while the Kapton serves as a wear plate. The twisted leads from the coils to the BNC connector are omitted for simplicity.

## OPERATIONAL PRINCIPLES

Figure 6 is a schematic of the basic units of this system. Figure 7 is a photograph of the actual equipment. Some descriptive details follow.

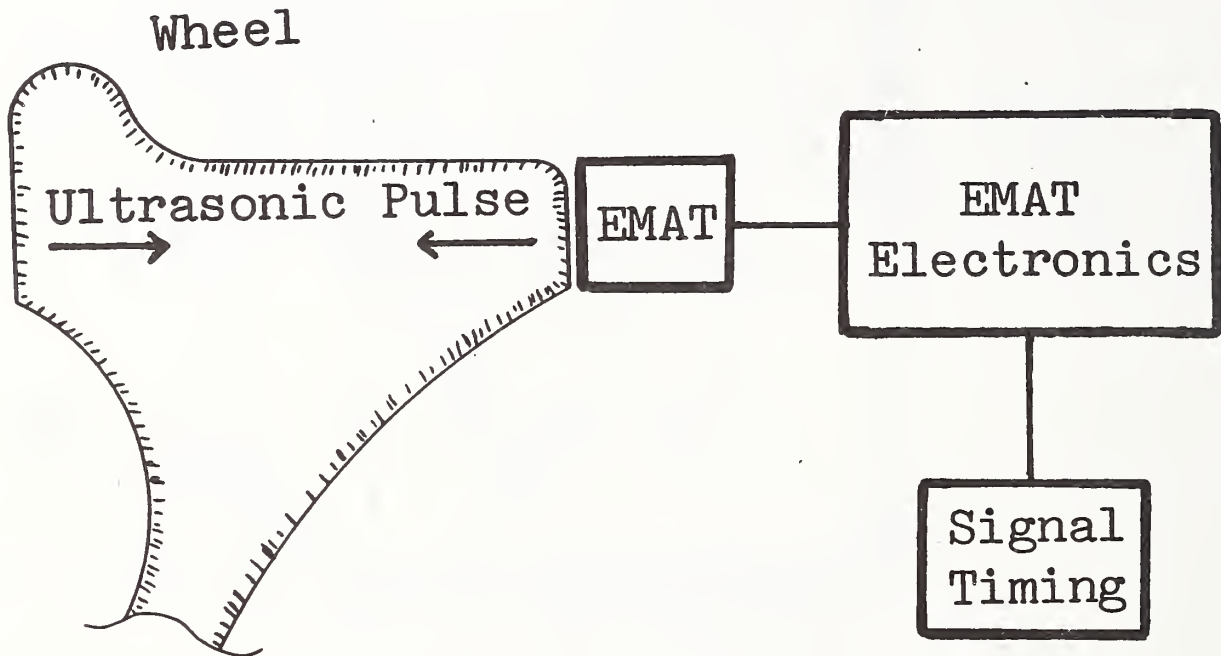


Figure 6. Block diagram of ultrasonic stress measurement system.

### Transducer Package and Fixture

The mechanical location of the EMAT on the front face of the wheel is very important (see **EXPERIMENTAL RESULTS**). To facilitate precise, rapid placement, we designed a fixture largely of polyester resin and fiberglass mat (Figs. 8 and 9). With this apparatus in position and adjusted (see **SYSTEM ASSEMBLY AND USE**), the aluminum cylinder with the EMAT is eased onto the wheel. Stops in the system allow rapid and accurate rotation between the two arrival time measurements.

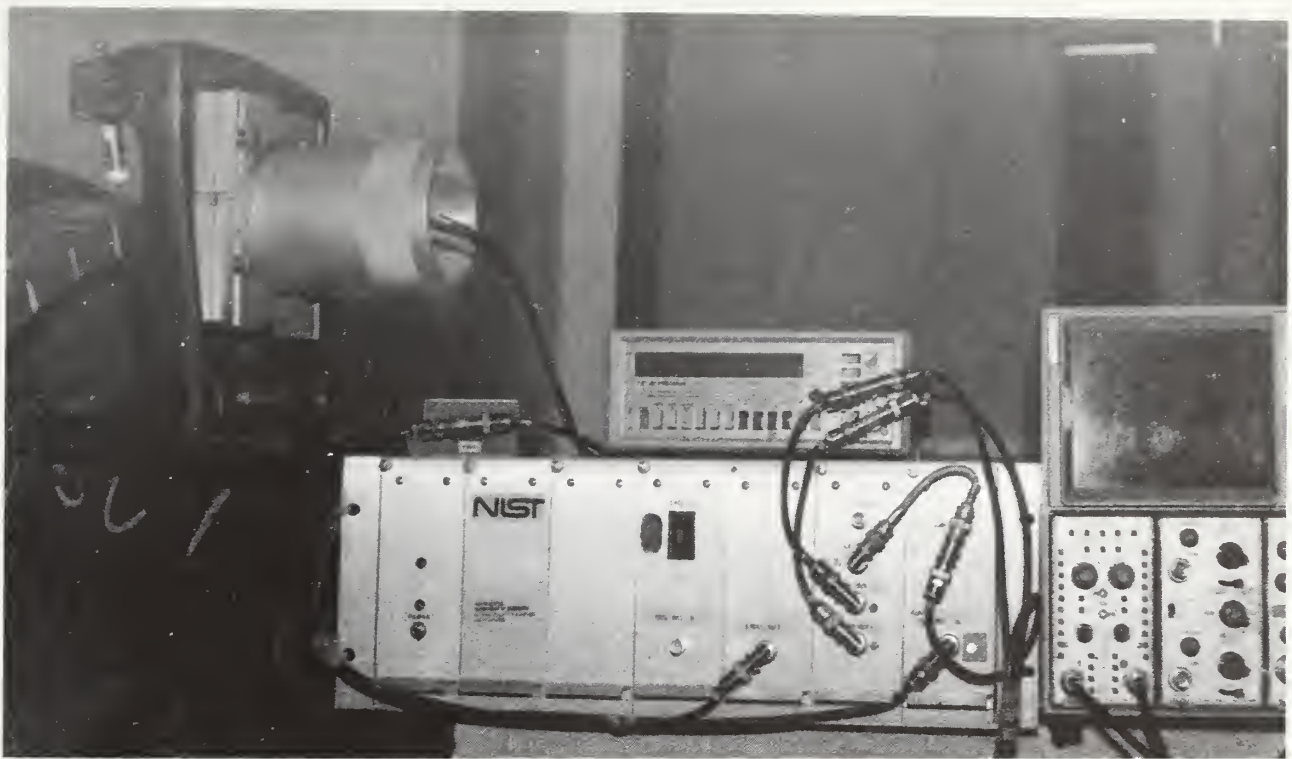


Figure 7. Photograph of the equipment represented in Fig. 6.

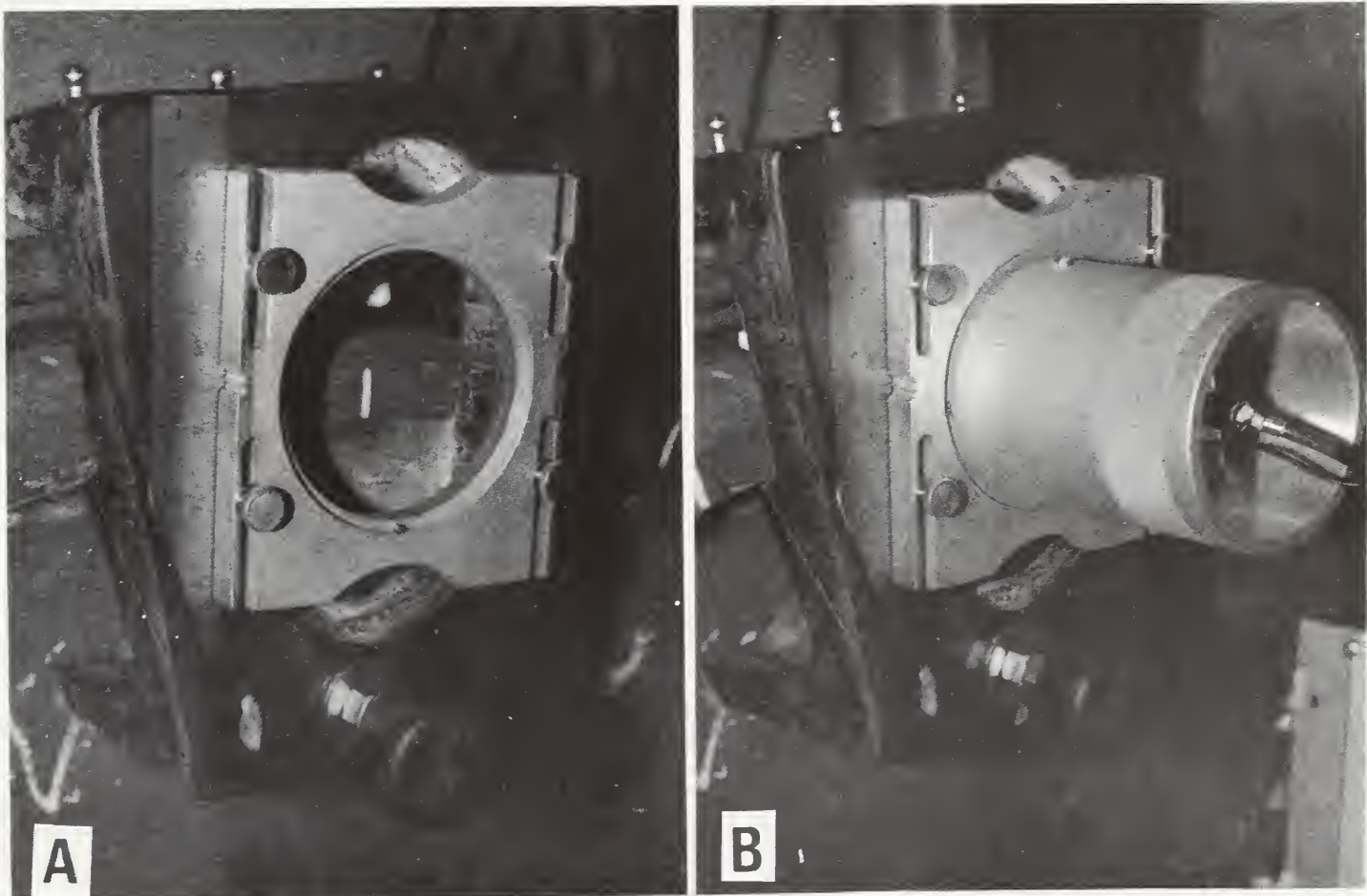


Figure 8. Close-up photographs of the wheel-mount fixture for the EMAT.  
A. The system attaches to the front face of the rim.  
B. The cylinder with the EMAT is then inserted.

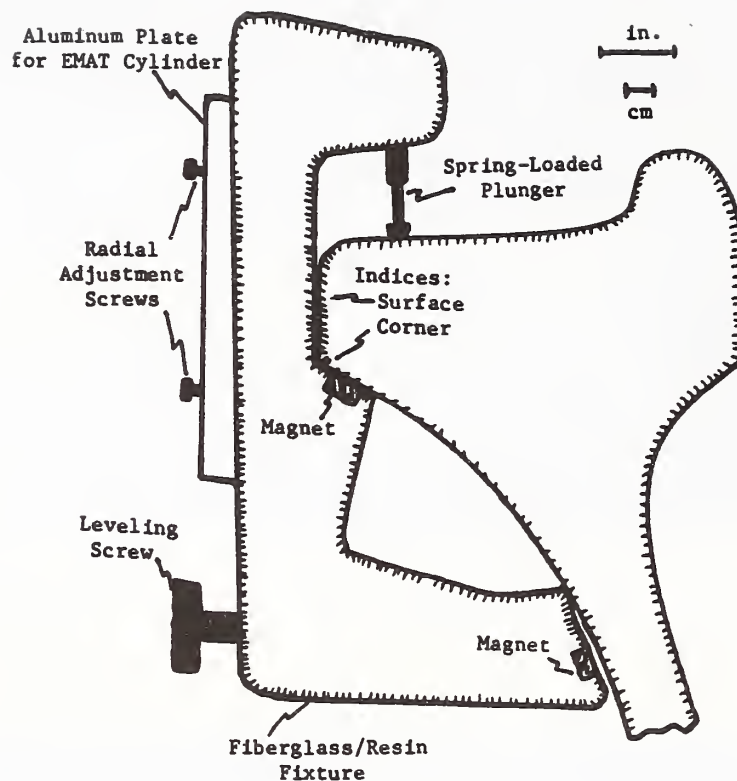


Figure 9. Schematic of wheel-mount fixture on a wheel rim (cf. Fig. 8). After adjustments for position and leveling, the EMAT cylinder is inserted in the top plate.

### EMAT Electronics

The first five modules of the electronics rack (Fig. 10) contain the power amplifier to generate the electronic pulse. This produces a gated pulse of power at 2 MHz. For all the results reported here, the number of cycles in the pulse was set at 10 with the thumbwheel in module 4. Figure 11 shows the voltage and current output as measured between the output of module 5 and the external matching circuit. The power amplifier operates at a pulse repetition frequency of 78 Hz. It generates a trigger with each pulse as a "start" signal for the interval timer and the oscilloscope.

Module 7 of the electronics rack is a high-gain, low-noise preamplifier for the received signal. The output goes to the digital gate and the oscilloscope. The gain is variable by screw adjustment through a hole in the front panel. Figure 12 shows a typical signal. Upon the initial pulse from the power amplifier, the preamplifier overloads and recovers after about 0.03 ms. The signals occurring at just less than 0.1 ms intervals are multiple acoustic echoes. On this time scale, the individual rf cycles are not evident.

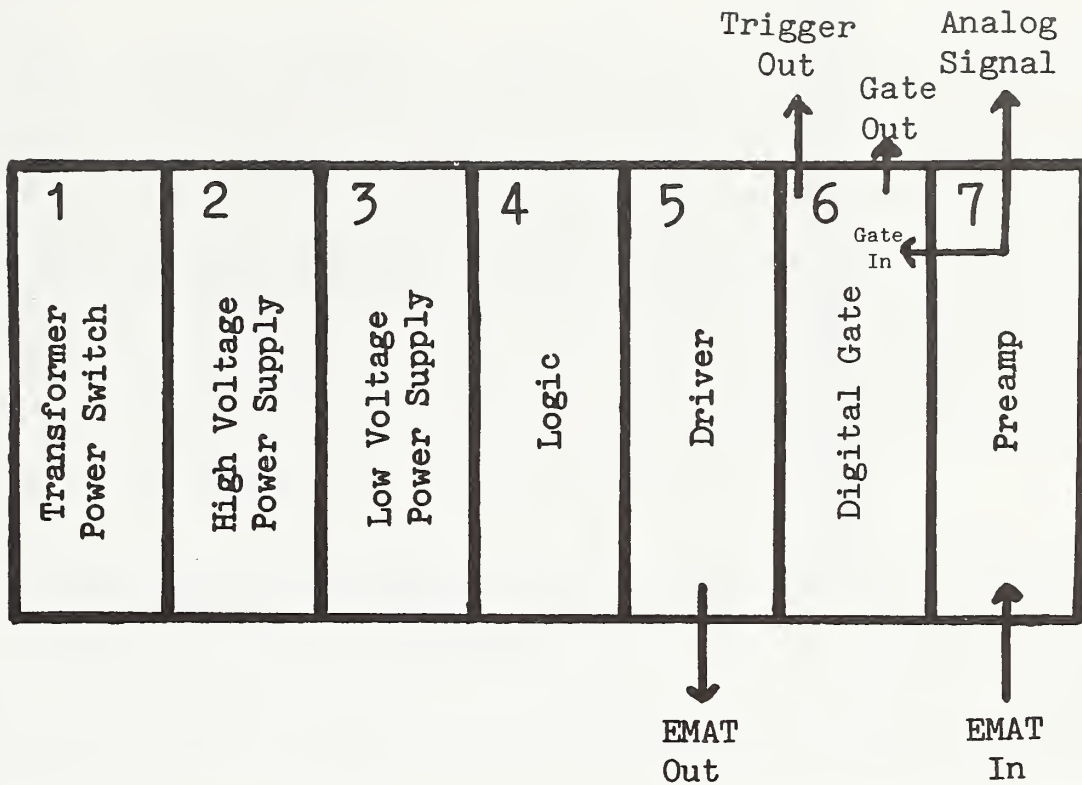


Figure 10. Identification of the seven modules in the main electronic unit. Coaxial cable connections go to modules 5-7. Input power is U.S. standard 110 V, 60 Hz.

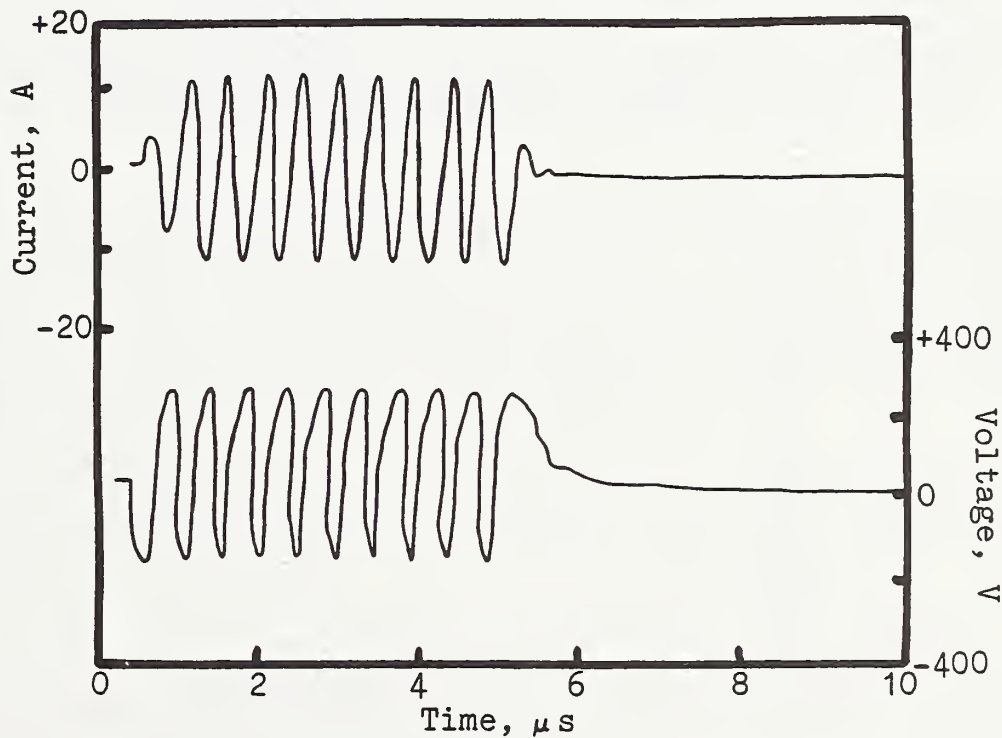


Figure 11. Voltage-current output of the power amplifier into the EMAT. This was measured between module 6 and the external matching network.

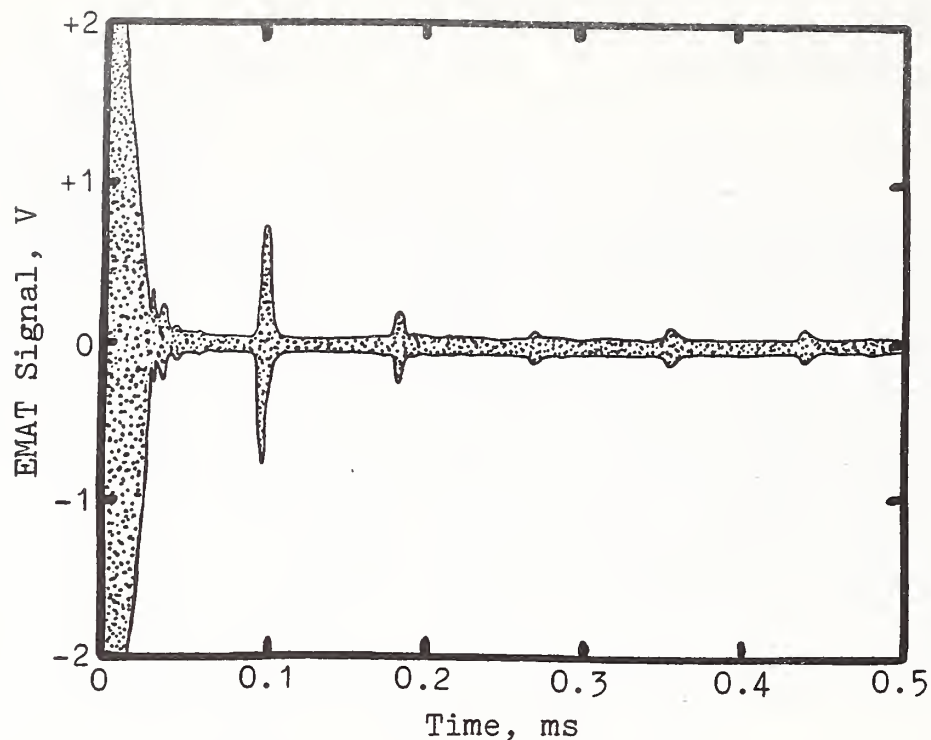


Figure 12. Oscilloscope picture of a typical signal from the pre-amp.

The box with the external matching electronics contains:

1. A diode expander circuit to prevent received signals from reflecting back into the power amplifier.
2. A low-pass filter to eliminate harmonics.
3. A series capacitor to tune the EMAT for resonance at 2 MHz. Figure 13 indicates both zero phase angle and a minimum in impedance to achieve maximum power transfer.

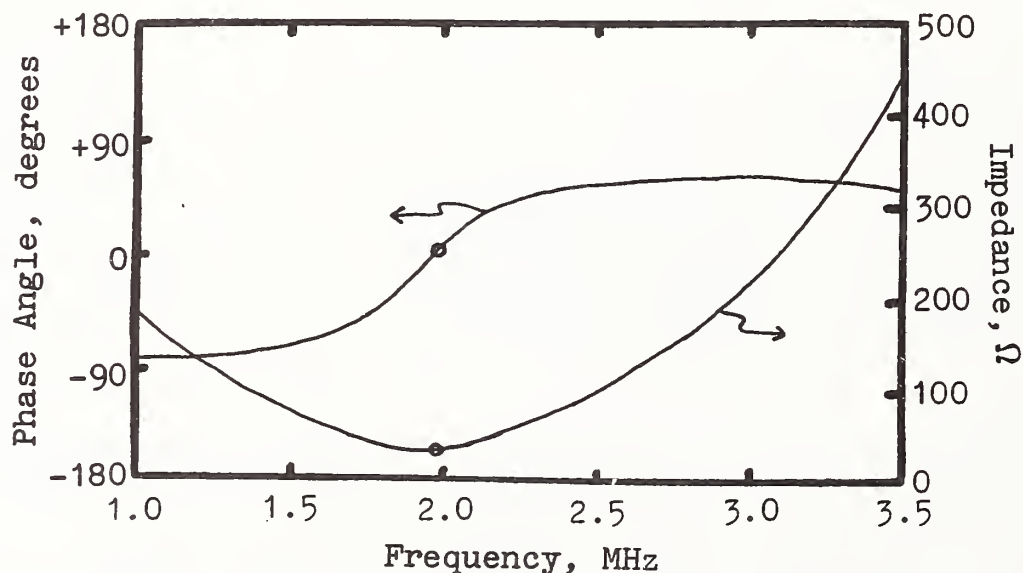


Figure 13. Impedance analyzer plot indicating resonance achieved by the tuning capacitor in series with the EMAT. This assures greatest power transfer and signal amplitude.

## Digital Gate

The digital gate located in module 6 (Fig. 10) is a special circuit that allows the high precision timing required by this procedure. It has coarse and fine controls (accessible through front panel holes) to adjust the time delay after the "start" trigger from the power amplifier. This roughly sets the two-way transit time of the ultrasonic signal through the rim thickness. After this delay, the gate looks for the next positive-going zero crossing that exceeds 100 mV. When this occurs, it generates a TTL pulse fed into the stop channel of the interval timer (see below). This makes it possible to time precisely the arrival of a selected cycle of the signal. Which cycle is chosen is unimportant as long as it is the same cycle for both polarizations. Usually, we select a cycle near the center of the signal packet where it is strongest and most easily identifiable.

The top BNC in module 6 is identified as the GATE MONITOR. This signal shows (on an oscilloscope) the allowed time window for the gate TTL pulses. At the time of initial set-up, displaying the acoustic signal and this monitor signal simultaneously allows adjusting the time delay so that the leading edge of the square pulse is near the center of the first echo. The final delay adjustment is easiest while looking at the individual TTL signals from GATE OUT.

In practice, we use the oscilloscope to observe the outputs of both the pre-amp and the digital gate. Figure 14 shows a typical scope display. In this case, the time base is greatly expanded around the arrival of the first echo, the top trace. The bottom trace is the gate signal which has been delayed to the arrival of the cycle at the center (cycle with the maximum amplitude). It is also possible to count the cycles from the beginning of the packet. The first TTL pulse acts as the "stop" signal; the subsequent pulses occur for each following cycle but are not used.

The gate delay is adjusted for the first of the time measurements and the EMAT is then rotated for the second measurement. In the event the TTL pulse then triggers at the preceding or following cycle, the arrival time will jump by the cycle period. For a 2 MHz signal, this is 500 ns and is much larger than what is usually due to birefringence. This large jump is a warning that the gate delay needs a minor adjustment.

It is also possible that the gate delay is just at an edge where the TTL pulse jumps back and forth between successive cycles of the acoustic signal. This condition has two symptoms:

1. The first TTL pulse of the GATE OUT trace will visibly jitter in time on the oscilloscope.
2. The readout from the interval timer will be very sporadic between successive averages (see below).

The remedy is to adjust the fine time delay until the gate locks onto the desired cycle.

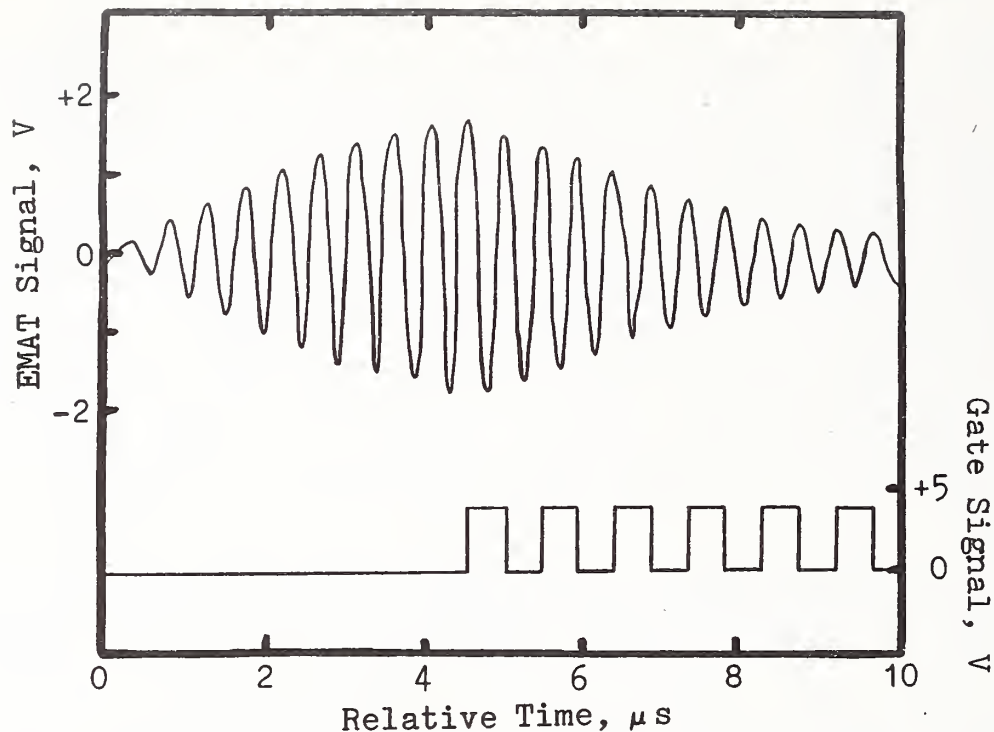


Figure 14. Oscilloscope trace expanded around the arrival of the first echo (top trace). The bottom trace is the digital gate output. The delay here places it at the center of the echo. The first TTL pulse stops the interval timer.

### Interval Timer

The instrument used to measure the echo arrival time is a commercial instrument [7] set to read to the nearest nanosecond. The "start" signal comes from the trigger of the power amplifier while the "stop" signal comes from the digital gate. To achieve maximum accuracy, we usually set the timer to average 100 readings; this renews the display every 1.3 s and the scatter in the displayed arrival time is usually  $< \pm 10$  ns (assuming proper adjustment of the time delay on the digital gate). Averaging 1000 times takes longer, obviously, but does yield very stable data.

The basic configuration (buttons pushed in) we have used is:

Left-to-right, bottom of panel -  
 Power  
 TI, A→B  
 .001 μs, RESOLUTION  
 Top-to bottom, right of panel -  
 Channel A (start) -  
 ×10  
 TRIG LEVEL, PRESET-IN  
 LPF  
 Channel B (stop) -  
 ×10

## SYSTEM ASSEMBLY AND USE

### Wheel Mount System

Since the railroad wheel tread wears and changes in profile, this fixture (Fig. 8) indexes on the wheel's front face surface and the corner where it turns into the wheel plate (Fig. 9). Spring-loaded plungers make contact with the tread; these and three magnets support the apparatus in place. The EMAT must maintain close coupling with the flat surface to produce a strong signal; therefore, there is a screw for fine adjustment of the plane of the transducer to assure it coincides with the rim face. The radial location of the EMAT is very important (see RESULTS); therefore, a top plate, which positions the transducer, has a limited range of travel in this direction and locks in place. Pointers in the plate and rulers on the fixture facilitate this adjustment. Experience with many wheels may (hopefully) show that this position will very infrequently need change, and measurements at one radial position will be sufficient.

An aluminum cylinder holds the EMAT box (Fig.5) fixed in place by set screws. After positioning the fixture, the operator slips this cylinder assembly into the hole in the top plate. There are mechanical stops 90° apart to facilitate rotation to the two polarization directions.

On the basis of limited practice, it seems that this device allows very repeatable time readings when it is removed from and replaced on a test wheel. Moving between the two rotations while maintaining exact location is very easy.

### Connections and Cables

The block diagram in Fig. 6 shows three functional units. These electronic components are in five discrete boxes:

1. EMAT
  - A. The EMAT, contained in a large aluminum cylinder.
2. EMAT Electronics
  - B. The large rack with seven modules.
  - C. The matching electronics in a small box.
3. Signal Timing
  - D. Time interval counter (commercial).
  - E. Oscilloscope with dual channels and expandable time base.  
(This is not part of the equipment delivered.)

Standard coaxial cables connect these five boxes. There are five major lines (Fig. 15), and we identified each of them with a color to make it easy to check or re-establish connections. There is a colored dot at each of the BNC's and a colored band around each end of the coaxial cables.

<u>Color</u>	<u>Connections</u>
White	EMAT OUT (module 5) → IN (external matching)
Copper	GATE IN (Module 6) → AMP OUT (module 7) → CH. 1 (scope)
Red	TRIG OUT (module 6) → CH. A (start, timer) → TRIGGER (scope)
Green	GATE OUT (module 6) → CH. B (stop, timer) → CH. 2 (scope)
Silver	EMAT IN (module 7) → OUT (external matching) → EMAT

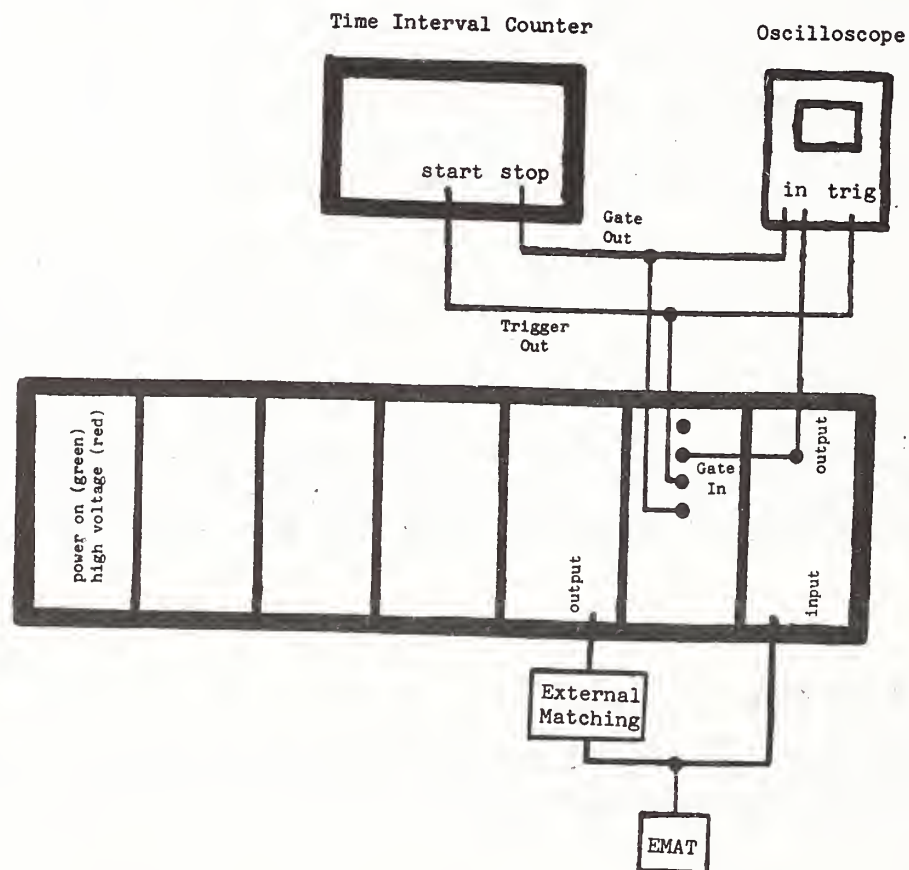


Figure 15. Interconnection of the electronic units by coaxial cable.

### Data Collection

To assure best accuracy, the interval timer should have a warm-up period of at least 15-30 minutes. After completing the physical positioning of the wheel fixture, placing the EMAT on the wheel rim, adjusting the gain of the signal amplifier (if necessary), and setting the gate of the digital timer, the operator can make the actual measurements quite rapidly.

1. Rotate the EMAT cylinder to one orientation (note arrow marked on transducer box to indicate polarization direction).

2. Observe interval timer readout. There will be some minor variation ( $\leq \pm 10$  ns) between successive readings; record a typical value.
3. Rotate the cylinder  $90^\circ$  to the second position and repeat step 2.
4. Repeat steps 1-3 several times (three to five) to increase confidence in readings.
5. Average the sets of readings in the two orientations. Discard any values that cannot be repeated.
6. Calculate the birefringence from eq. (1).
7. Subtract the proper value of the texture birefringence for the radial position (see RESULTS), and calculate the stress from eq. (2).

The following is a typical data set:

	Arrival Times, $\mu\text{s}$		B ( $10^{-4}$ )	Stress ( $\sigma_\theta - \sigma_R$ )	
	Radial	Circumferential		MPa	ksi
(Rim block measurement to determine $B_0$ , or birefringence due to texture - generally, this value will be a previously known average of measurements such as this)					
	94.042	94.143			
	94.043	94.144			
	94.040	94.145			
Avg.	94.042	94.144	-10.8 (= $B_0$ )		
(Wheel measurement to determine B, or total birefringence)					
	90.920	90.931			
	90.917	90.934			
	90.919	90.934			
Avg.	90.919	90.933	-1.5	-130	-19

Since the stress in the radial direction is generally negligible, this example indicates a small compressive hoop stress. The magnitude of the arrival times depends on the exact thickness of the rim. It is the fractional change between polarizations that is important.

## EXPERIMENTAL RESULTS

### EMAT/PZT Comparison

An early collaboration [8-11] with Prof. H. Fukuoka of Osaka University compared measurements made with electromagnetic and more conventional piezoelectric transducers.

The measurements made with the two systems were the same within experimental error. One important difference did emerge, however. To achieve good

acoustic coupling between the PZT device and the wheel rim, it was necessary to mill a flat area on the rim, while the EMAT could operate over a rusted, pitted surface. This has obvious advantages for field use where the EMAT may require only modest wire-brushing to knock loose debris from the test surface. Figure 16 indicates the comparability of a number of measurements. The EMAT/PZT difference is smaller than the expected experimental error.

Figure 16 also confirms an earlier finding that the degree of birefringence is strongly dependent on the radial position of the transducer [6]. Figure 17 shows the convention used here. The zero position was at the approximate center of the width of the front rim face. Negative distances indicate positions closer to the axle, while positive distances mean sites nearer the tread. This position dependence is small, but, since it is comparable to the size of the effects of interest, it is essential that the position be carefully controlled. Some possible causes of this effect are signal interaction with the tread surface, the strong variation of the metallurgical texture (see Texture Measurements below), or a significant gradient in the stress state.

These small shifts between measurements meant exerting considerable care in placing the transducers. The main reason for the eventual construction of the wheel mounting fixture for the EMAT was to speed up this process while making it easier and more reliable.

### Stress Sensitivity

Previous work [6,12] had shown the sensitivity of acoustoelasticity to the stress state. However, Dave Utrata at the Association of American Railroads Technical Center in Chicago lent us a pair of test wheels to demonstrate this effect in yet another way. While the wheel stress characterization was not sufficient to quantify or calibrate our measurements, the data did display the known and expected characteristics.

Both wheels had a saw cut along a radius, from tread to hub. At the outer (tread) end, there was a larger cut-out to accommodate the actuator of a small hydraulic press. With a hand-operated pump, it was possible to spread two sides of the wheel rim apart and introduce a hoop compressive load. For the measurements plotted in Fig. 18, the EMAT was positioned 180° from the actuator. After pumping the hydraulic pressure to predetermined levels, the ultrasonic wave transit time measurements were made at several radial positions.

The plots in Fig. 18 reveal several characteristics:

1. The birefringence increases with higher pump pressure or greater compressive stress. Using the sign conventions of eqs. (1) and (2), this confirms that  $C_A$  is negative.
2. If we assume that the rim hoop stress is linear with the pump pressure, Fig. 4 shows the stress is also linear with the birefringence, as per eq. (2). All the data sets have the same slope or  $C_A$ .

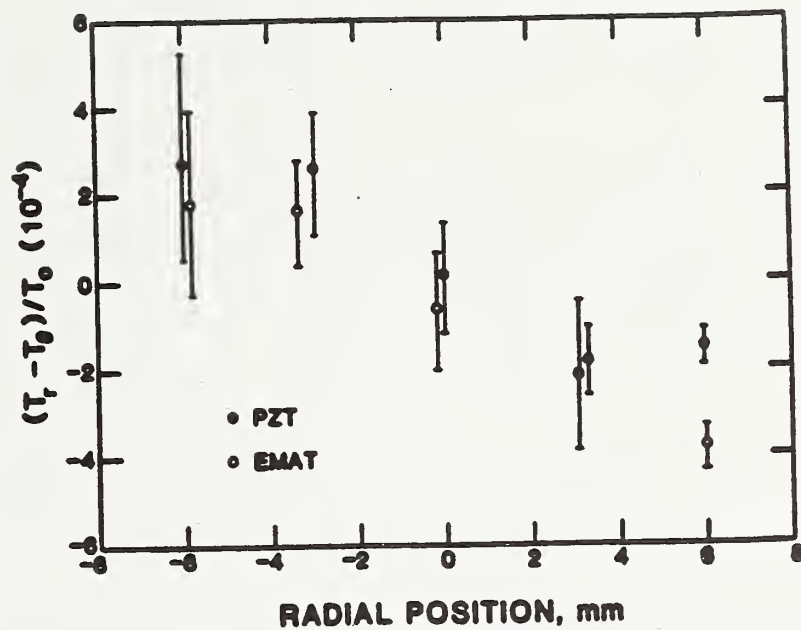


Figure 16. Comparison of measurements using two types of transducers at several radial positions on a wheel rim face. The error bars indicate the standard deviation of the measurements.

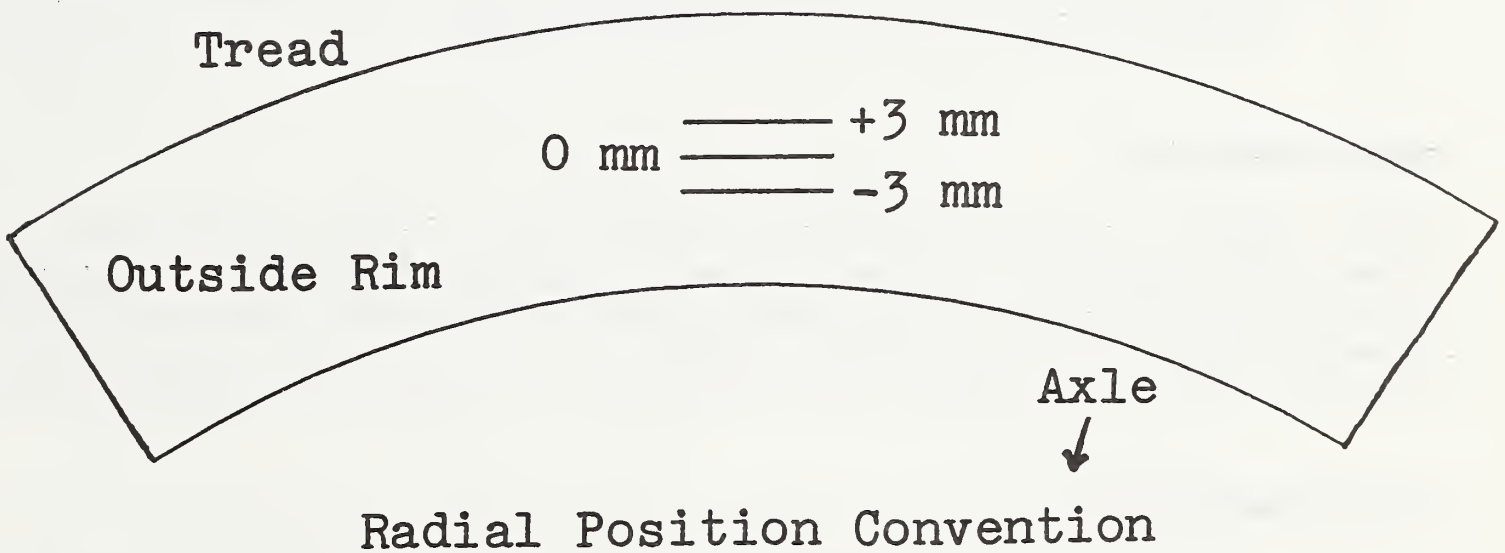


Figure 17. This is the convention for radial position used in the work. The zero position is at about the mid-line of the front face. Negative positions are closer to the axle, while positive ones are closer to the tread.

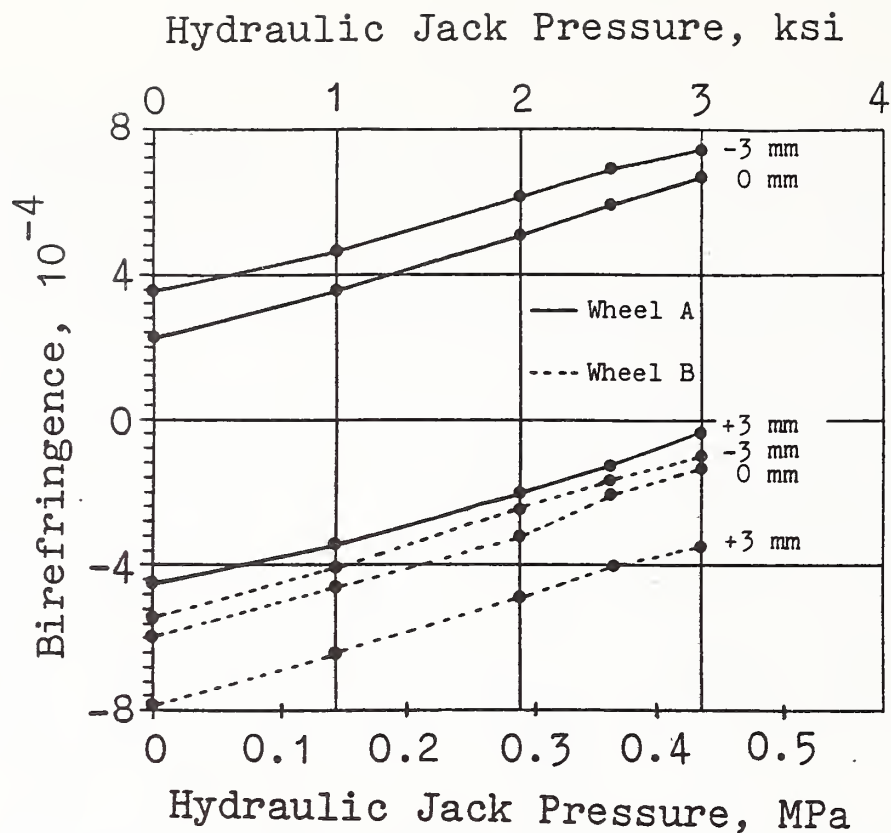


Figure 18. Birefringence in two AAR test wheels as hydraulic pressure is applied to generate compressive hoop stress. The ultrasonic tests were made at three radial positions on each wheel.

3. The zero-pressure measurements from the two wheels are considerably different. This is most likely due to different residual stresses still remaining after the one radial saw cut. They also likely have a different underlying metal texture since they are different classes.
4. Again, there is a strong radial dependence, with the most negative birefringence occurring nearest the tread.

#### Saw-Cut Comparison

Earlier reports of measurements on an intact wheel [7,10] indicated the presence of compressive residual stress in the rim. Subsequent saw cutting at TTC gave qualitative, if not quantitative, confirmation when the wheel closed on the saw blade during the cutting.

#### Texture Measurements

As noted previously, the metallurgical texture of the specimen contributes a significant fraction of the measured birefringence. This must be taken into account when calculating the stress, eq. (2). If the specimen is available before being stressed or there is always an unstrained reference specimen available that contains the same texture, the problem is simply to make two measurements and subtract. In practice, this is seldom possible--never for in-use tests of railroad wheels.

The photographs in Figs. 19 and 20 indicate the type of texture produced by casting. These are the result of polishing and macroetching a thin slice from the rim of a wheel taken from service. There is a very prominent dendritic structure growing normally from each exterior surface. The dendrites are about 20-25 mm long as the result of grain growth during cool-down after casting. This large structural gradient is a graphic indication of the importance of establishing a fixed EMAT position before making the timing measurements.

To help learn the magnitude of the texture problem as a prelude to working on a solution, TTC sent us two rim blocks each from ten different wheels. All of the wheels were manufactured by Griffin, but they were fabricated by four different plants. The rim blocks were about 20 cm long and nominally free of bulk residual stress. The measurements on these are in Fig. 21, grouped by production plant. Figure 22 combines the four data sets.

Figure 22 gives a worst-case indication of the data scatter. A simple average of the values is  $\approx -5 \times 10^{-4}$  with a spread ( $\delta B_0$ ) of  $\pm 5 \times 10^{-4}$ . This translates to a stress uncertainty ( $\delta B_0/C_A$ ) of  $\pm 71$  MPa (10 ksi). Figure 21, however, indicates two possible refinements of this process:

1. Take into account the plant of origin (known from wheel ID markings).
2. Allow for the variation with radial position by curve fitting each plant's data (probably with a simple line).

With these procedures and a larger data base, it is possible to cut the texture uncertainty by a factor of almost 2.

While considerably more data are necessary, these initial measurements are a positive indicator that this approach will have sufficient accuracy and sensitivity to become a useful tool.

## ELECTRONIC CIRCUITS

Figures 23-31 are the schematics for the stress measurement system, comprised of five modules for the power amplifier, one module for the digital gate, one module for the signal pre-amp, and an external box with the matching electronics. The following list identifies all the components.

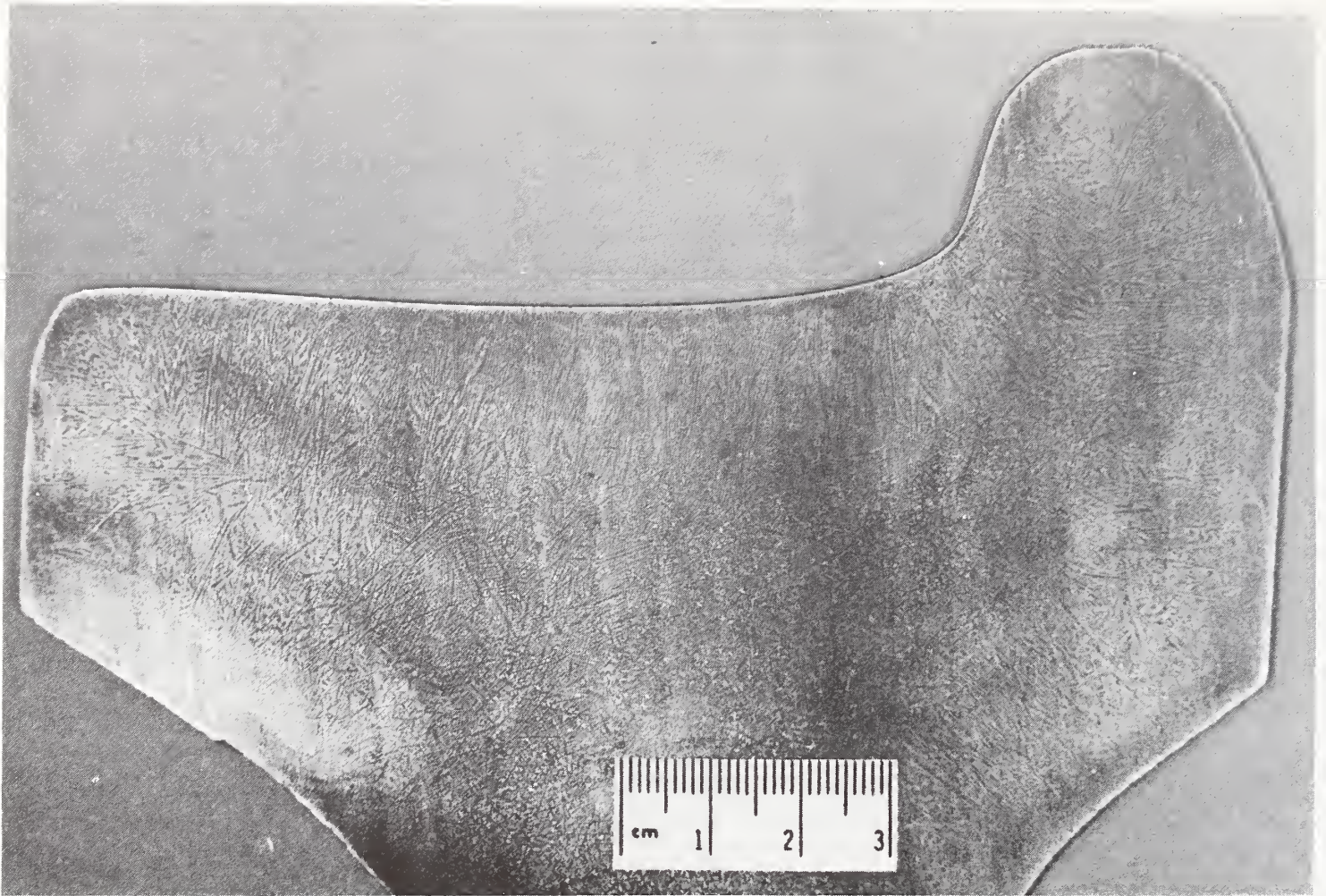


Figure 19. Cross section of a wheel rim after polishing and macroetching. Note the dendritic structure that has grown from each surface.

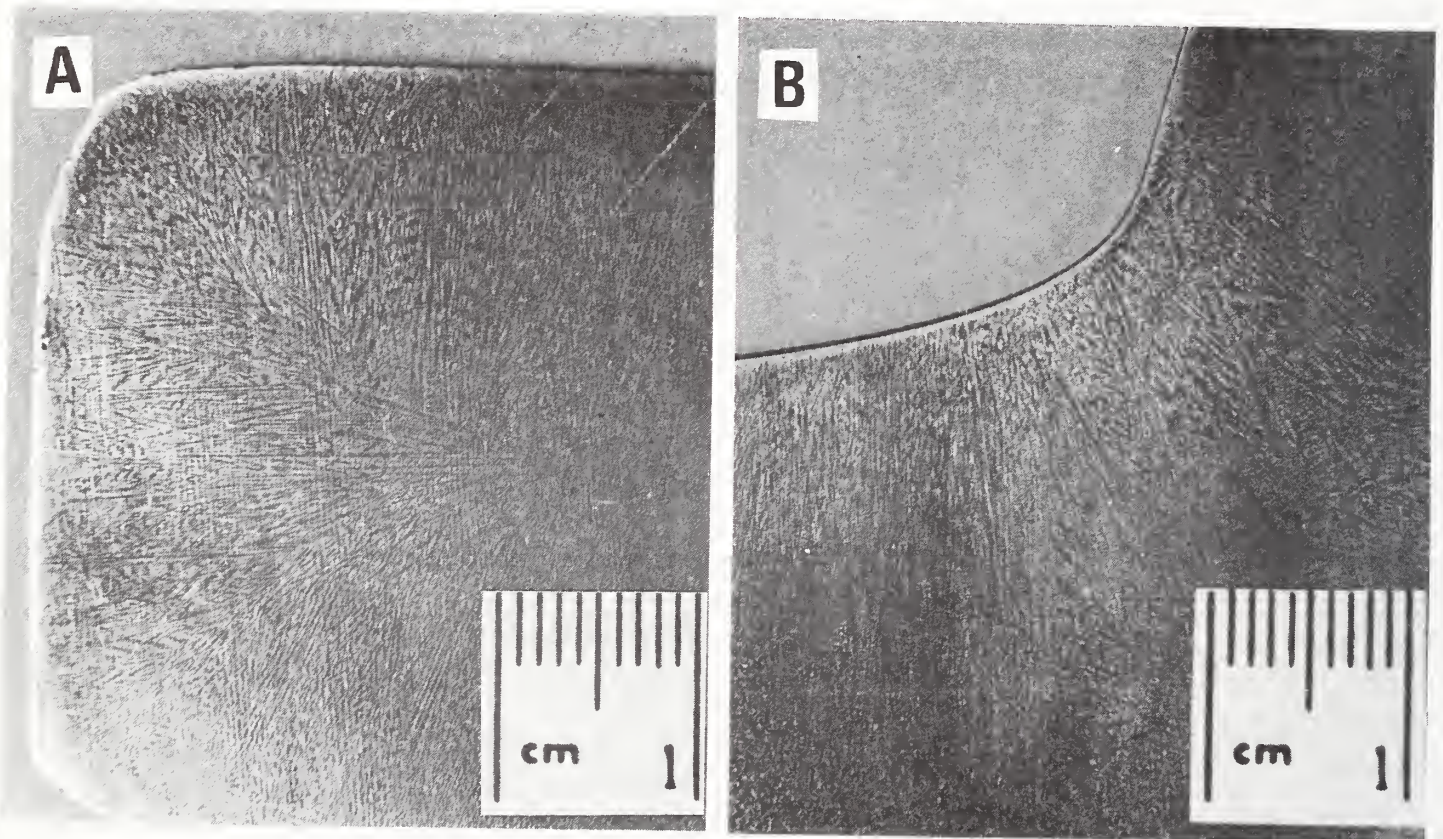


Figure 20. Enlarged view of macrostructure in Fig. 19.  
A. Front face of rim.  
B. Root of flange.

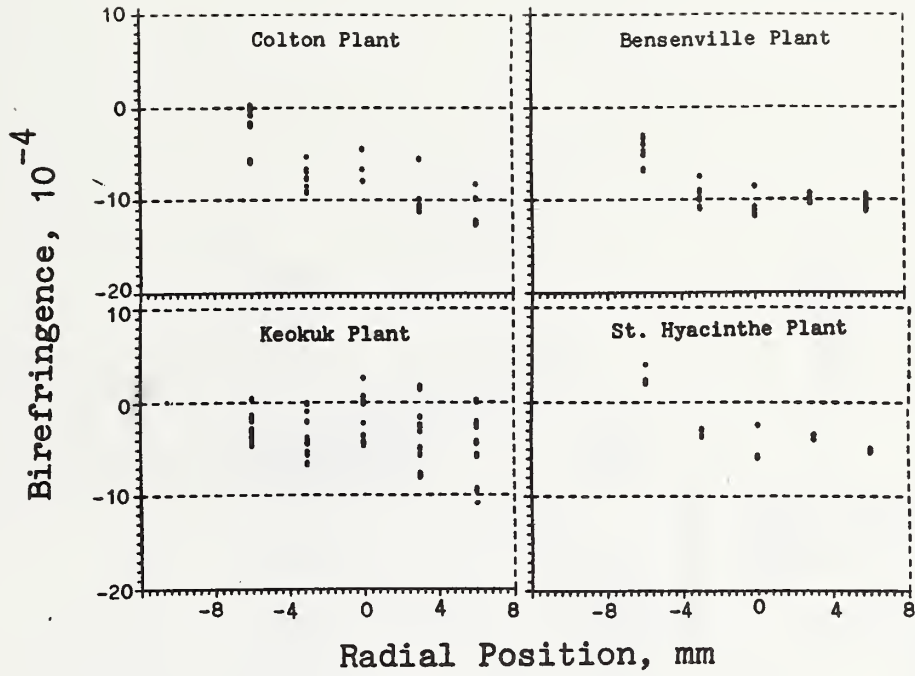


Figure 21. Birefringence measured on rim blocks from four production plants. The effect here is due solely to the metallurgical texture. There appear to be characteristic differences. An expanded data base is necessary to refine these trends.

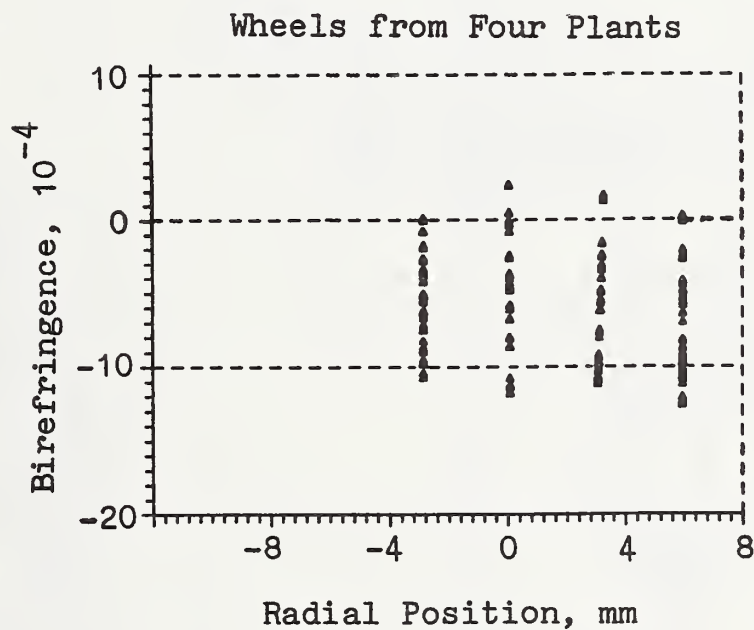
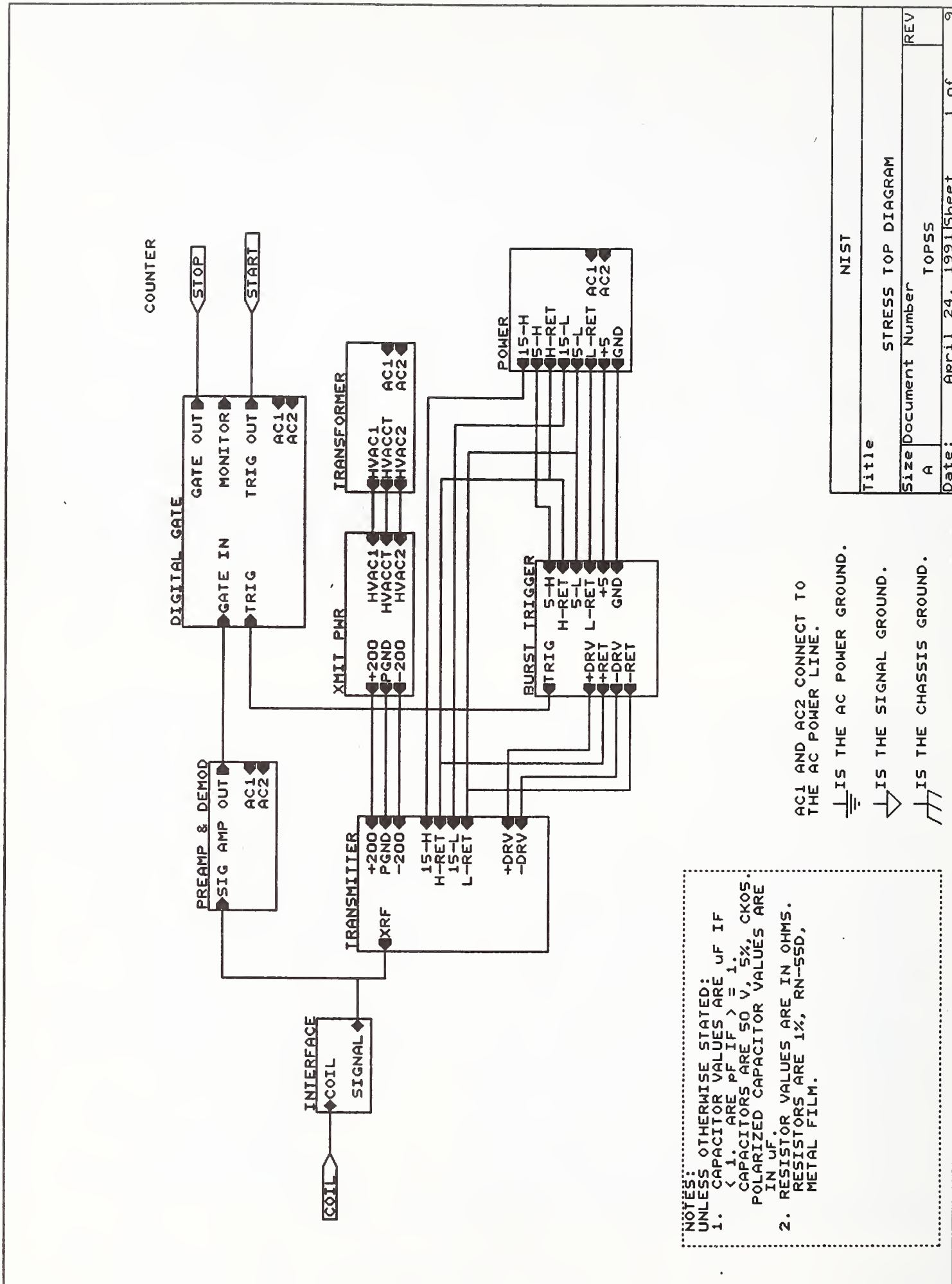
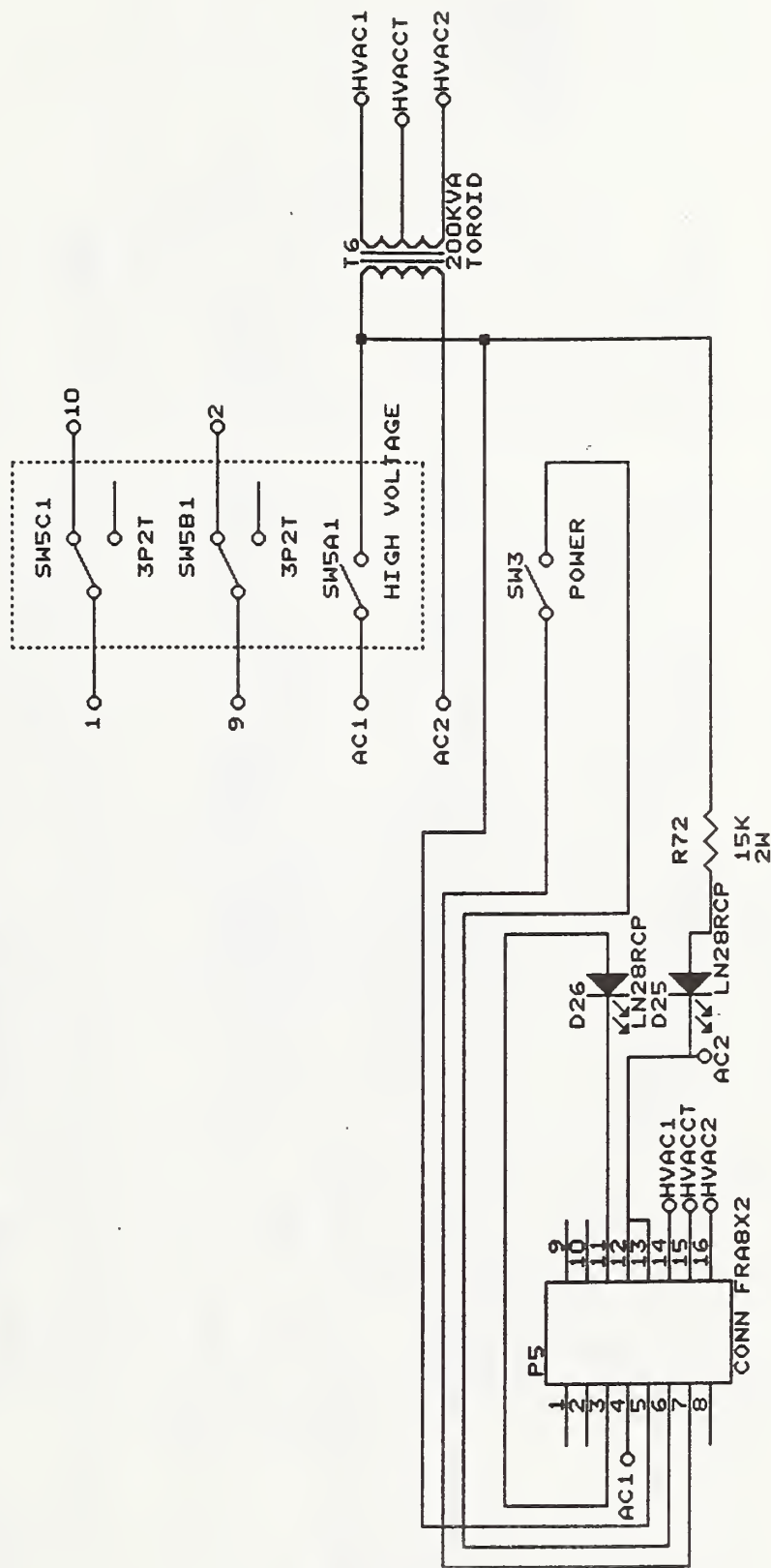


Figure 22. Collection of all the data in Fig. 21. Even in this worst-case scenario, with no knowledge of wheel's origin, the uncertainty in the texture is still within acceptable limits.



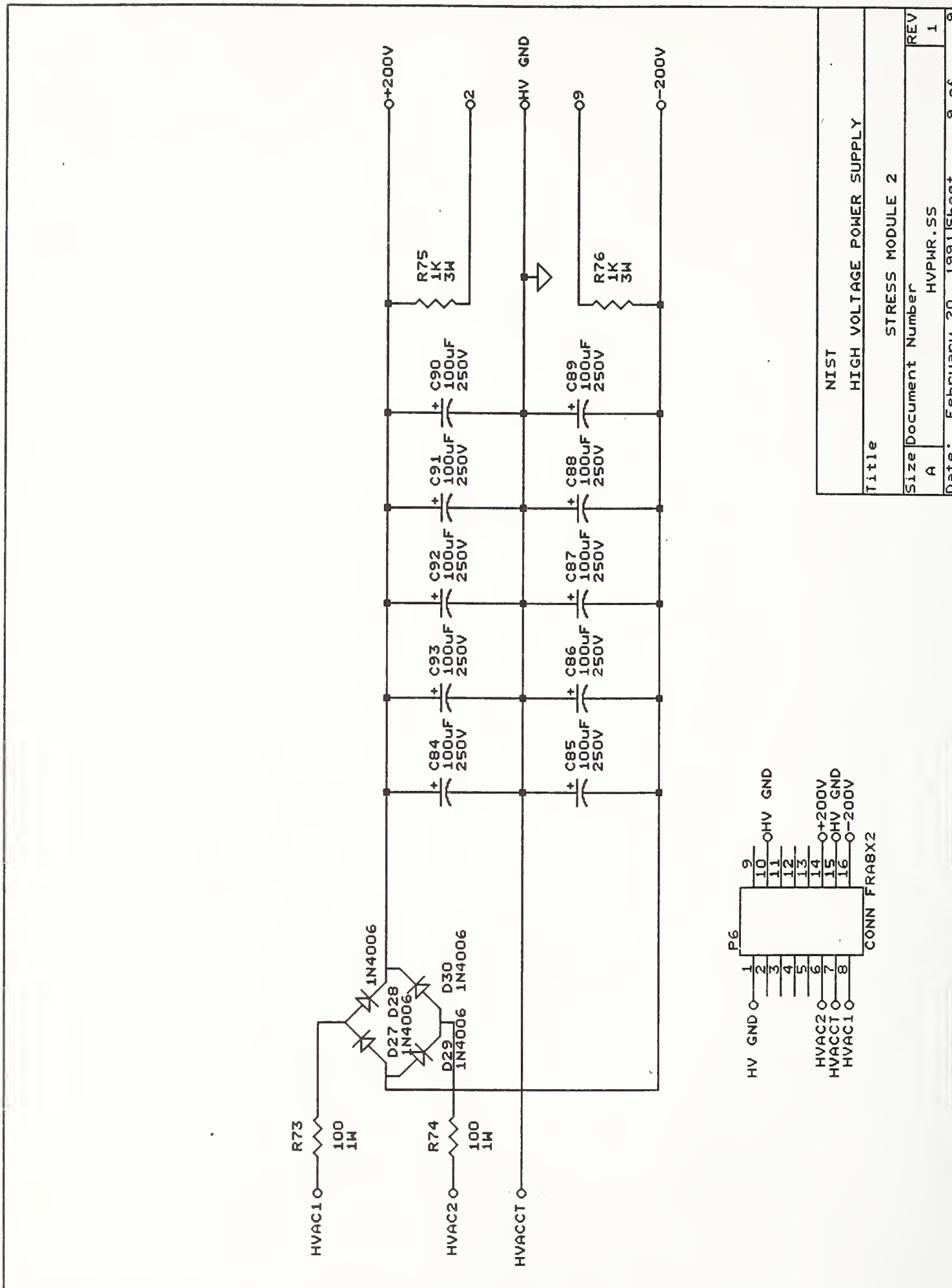
Title		NIST	
Size		STRESS TOP DIAGRAM	
Document Number	A	TOPSS	REV
Date:	April 24, 1991	Sheet	1 of 9

Figure 23. Power and signal connections in the main electronic unit.



Title		NIST	
Size		FRA MODULE 1	
Document Number		HVXFM.R.FRA	
REV	1	Date:	April 24, 1991
		Sheet	8 of 9

Figure 24. Transformer and power switches in module 1, main electronic unit.



Title	
NIST HIGH VOLTAGE POWER SUPPLY	
Size Document Number	
A	HVPR.55
Date: February 20, 1991	
Sheet	9 of 9
REV	
1	

Figure 25. High voltage power supply in module 2, main electronic unit.



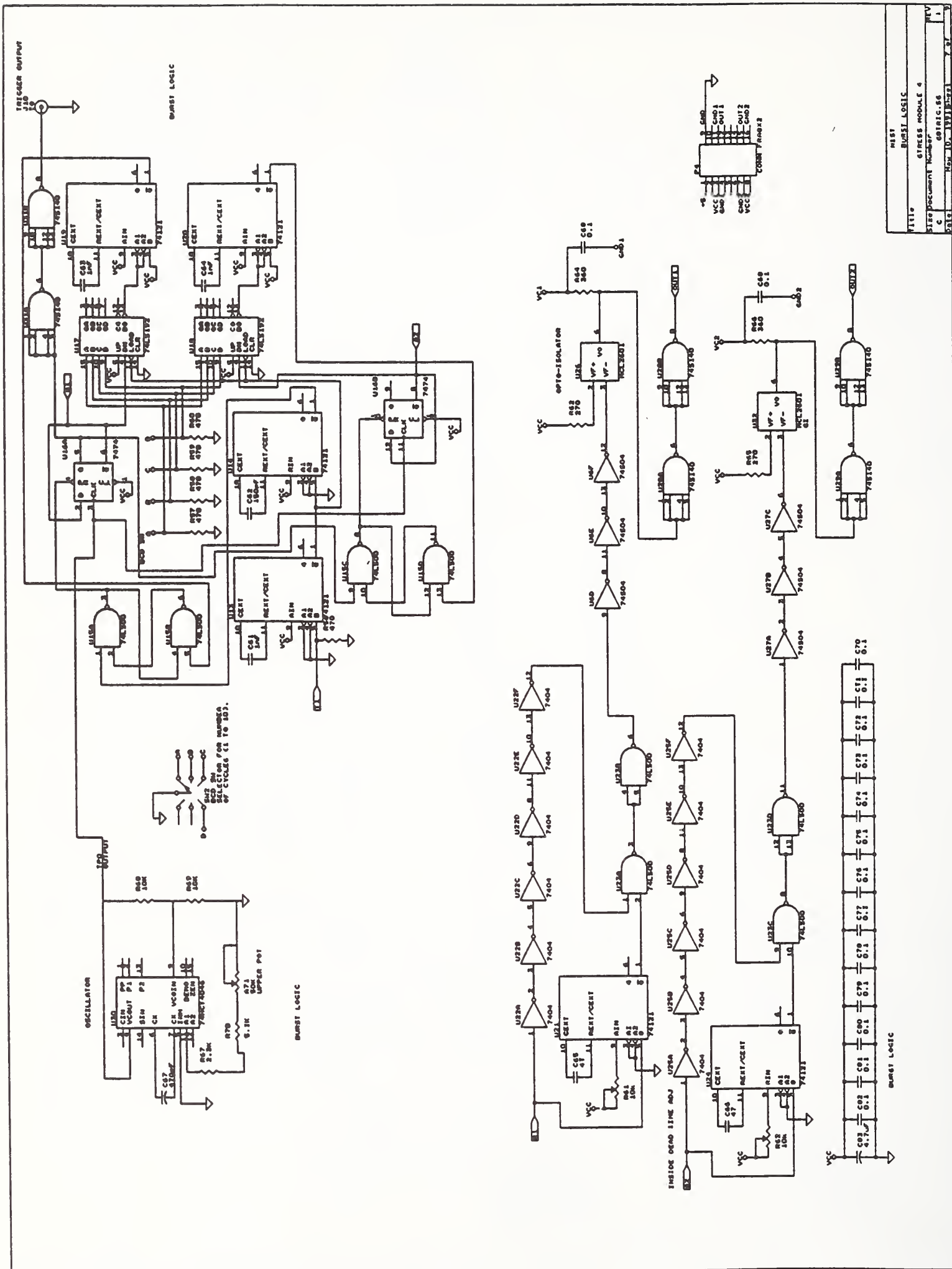
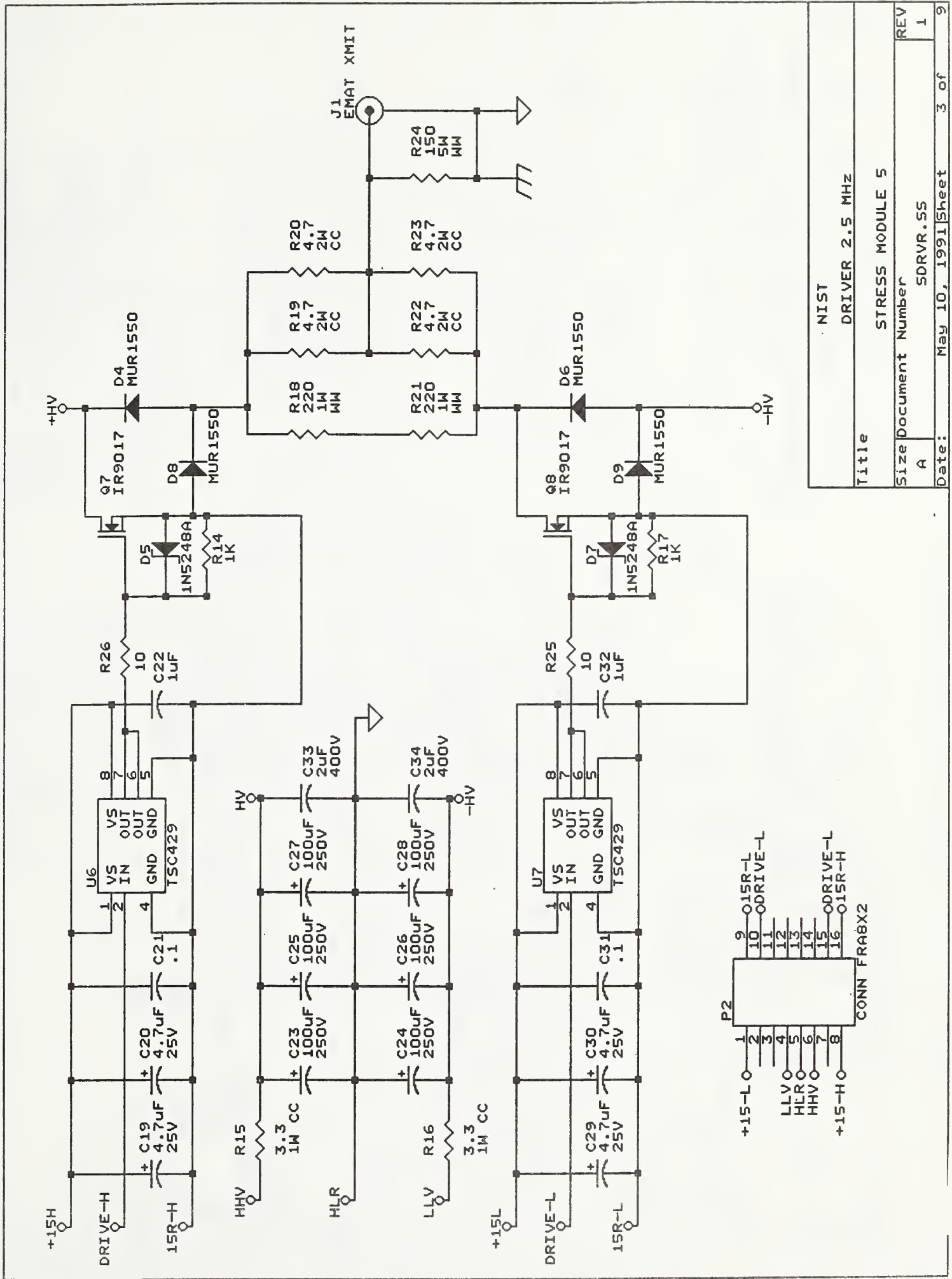
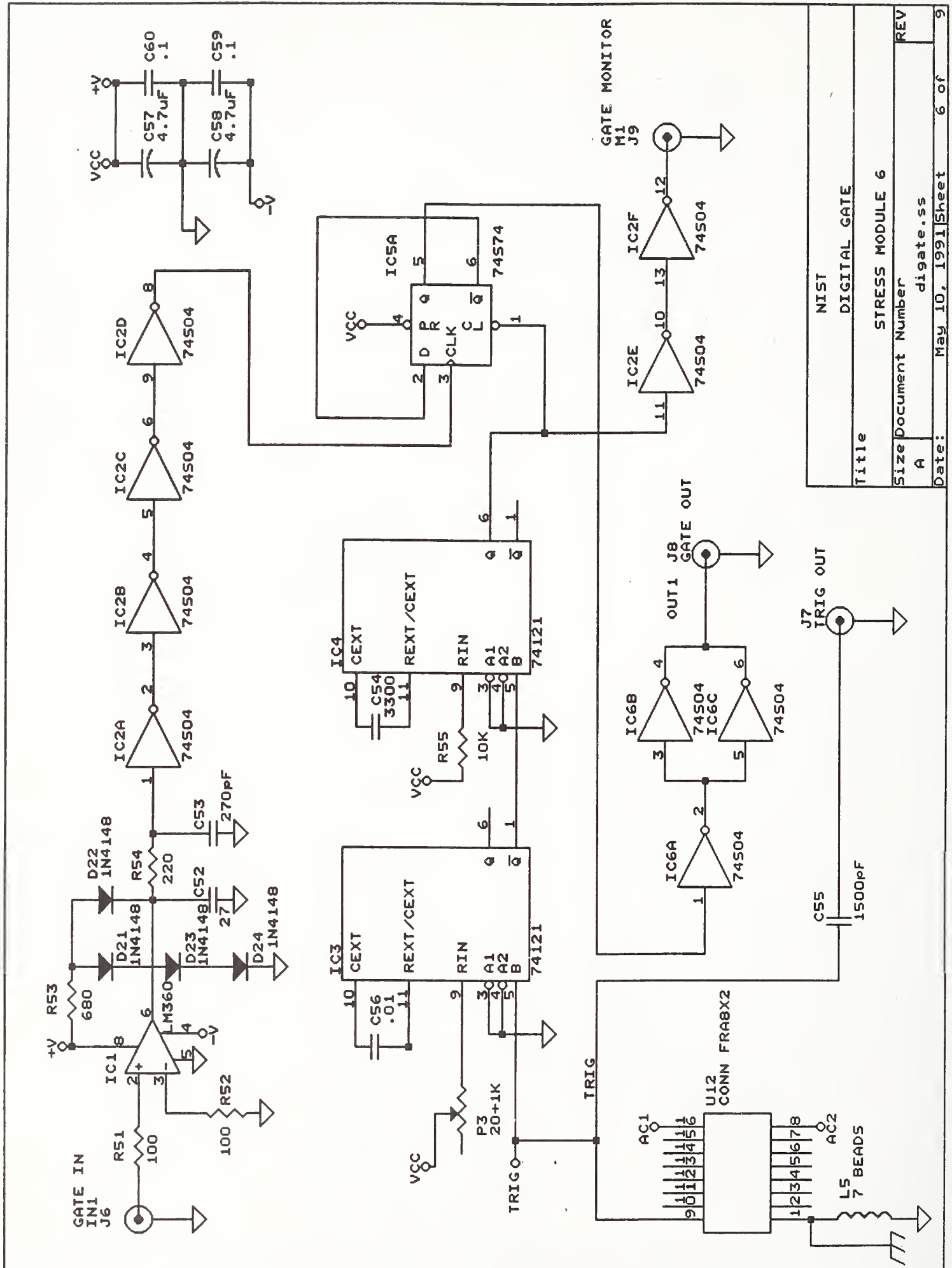


Figure 27. Burst logic in module 4, main electronic unit.



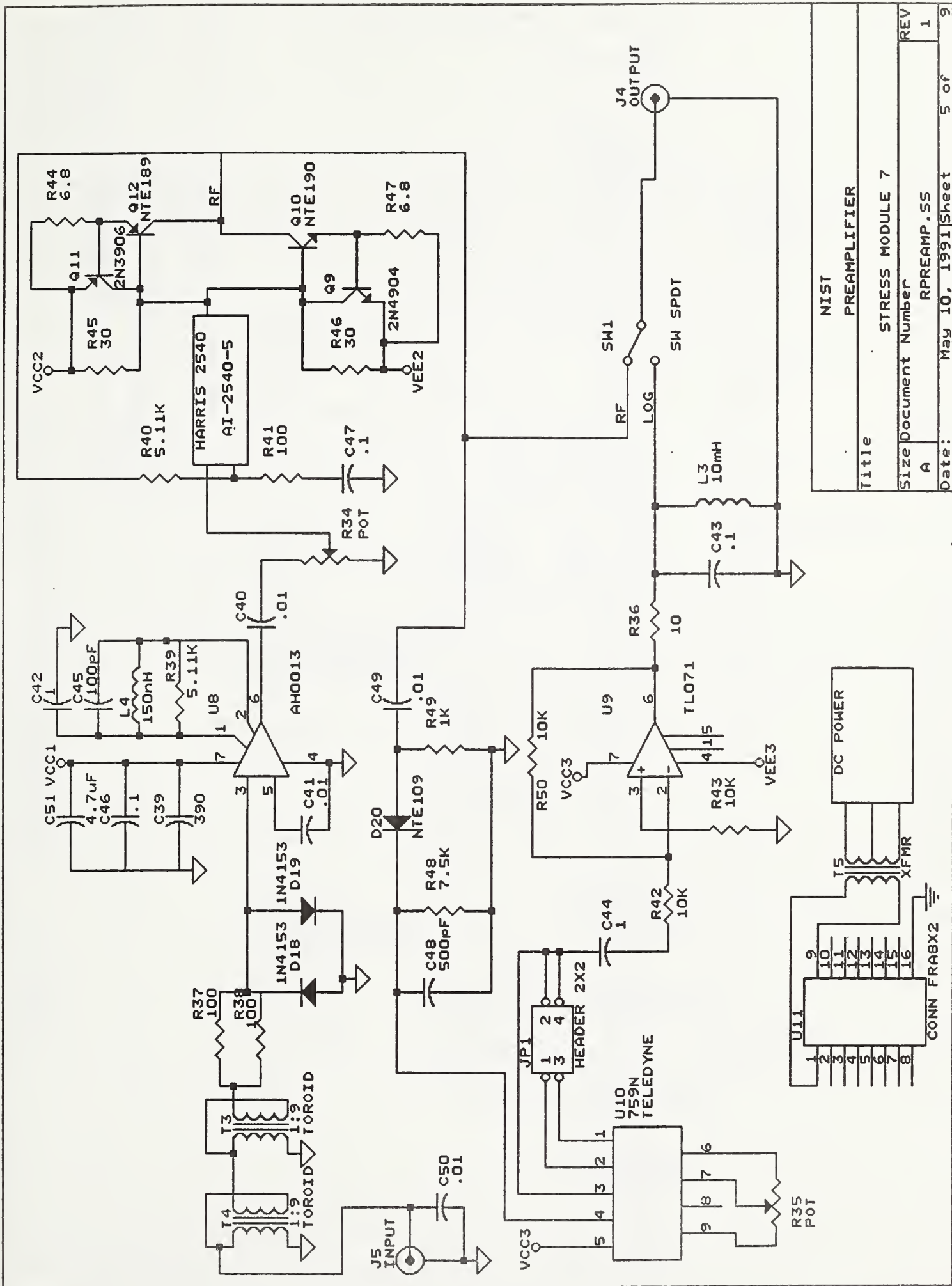
Title		NIST DRIVER 2.5 MHz	
Size		A	
Document Number		SDRVR.55	
REV		1	
Date:		May 10, 1991	
Sheet		3 of 9	

Figure 28. High power driver in module 5, main electronic unit.



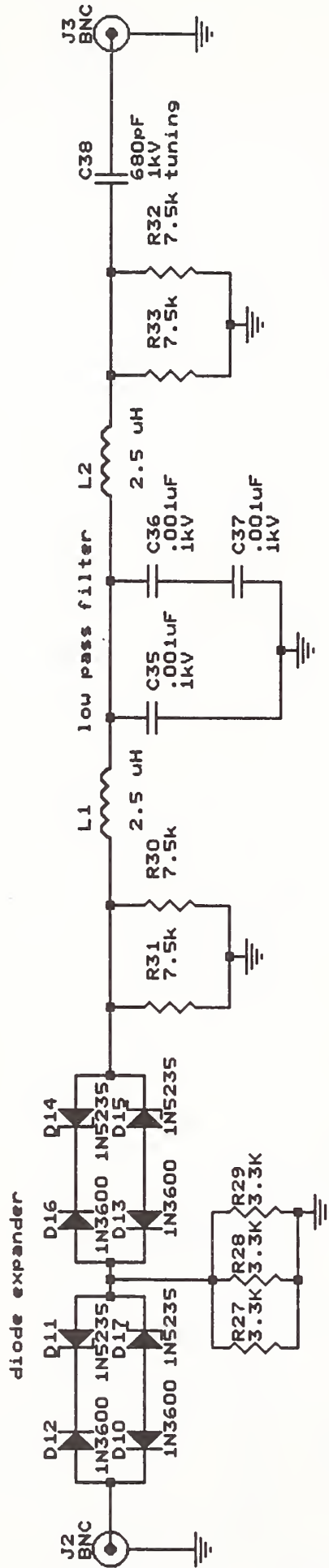
Title		NIST DIGITAL GATE
Size Document Number		STRESS MODULE 6
A	REV	digate.ss
Date:	May 10, 1991	Sheet 6 of 9

Figure 29. Digital gate in module 6, main electronic unit.



Title		NIST PREAMPLIFIER	
Size		A	
Document Number		STRESS MODULE 7 RPREAMP.SS	
Date:		May 10, 1991	
Sheet	5	of	9
REV	1		

Figure 30. Signal preamplifier in module 7, main electronic unit.



Title		NIST	
Size		EXTERNAL STRESS BOX	
Document Number		A	
Date:		April 23, 1991	
Sheet		4 of 9	
REV		INBOX.SRS	

Figure 31. Matching electronics in external box.

## List of Electronic Components

Item	Quantity	Reference	Part	Item	Quantity	Reference	Part
1	3	U1,U2,U4	LM723	37	4	R30,R31,R32,R33	7.5k
2	4	C1,C2,C6,C11	1000	38	3	C36,C35,C37	.001uF
3	1	R1	500	39	1	C38	680pF
4	1	R2	750	40	1	U8	AH0013
5	3	R3,R5,R10	5.6K	41	1	U9	TL071
6	12	C5,C8,C10,C13,C15,C21, C31,C43,C46,C47,C59,C60	.1	42	1	C39	390
7	1	R4	820	43	5	C41,C40,C49,C50,C56	.01
8	2	U3,U5	LM7805	44	2	C42,C44	1
9	7	R6,R11,R14,R17,R49,R75, R76	1K	45	2	R34,R35	POT
10	2	R7,R12	3K	46	1	JP1	HEADER 2X2
11	6	R8,R13,R27,R28,R29,R67	3.3K	47	1	U10	759N
12	1	R9	2.2K	48	7	R37,R38,R41,R51,R52,R73, R74	100
13	3	D1,D2,D3	NTE168	49	2	R39,R40	5.11K
14	4	T1,T2,T1B1,T2B1	FP34-340	50	6	R42,R43,R50,R55,R68,R69	10K
15	7	P1,P2,P4,P5,P6,U11,U12	CONN FRA8X2	51	2	R44,R47	6.8
16	3	Q2,Q4,Q6	2N2222	52	2	R45,R46	30
17	3	Q5,Q1,Q3	2N6122	53	1	R48	7.5K
18	6	C16,C17,C18,C61,C63,C64	1nF	54	1	D20	NTE109
19	14	C3,C4,C7,C9,C12,C14,C19, C20,C29,C30,C51,C57,C58, C83	4.7uF	55	1	Q9	2N4904
20	2	U6,U7	TSC429	56	1	Q10	NTE190
21	4	D4,D6,D8,D9	MUR1550	57	1	Q11	2N3906
22	2	D5,D7	1N5248A	58	1	Q12	NTE189
23	2	R15,R16	3.3	59	2	T3,T4	1:9
24	1	J1	EMAT XMIT	60	1	SW1	SW SPDT
25	2	Q7,Q8	IR9017	61	1	J4	OUTPUT
26	3	R18,R21,R54	220	62	1	J5	INPUT
27	1	R24	150	63	1	T5	XFMR
28	3	R25,R26,R36	10	64	2	D18,D19	1N4153
29	4	R19,R20,R22,R23	4.7	65	1	L4	150nH
30	16	C23,C24,C25,C26,C27,C28, C84,C85,C86,C87,C88,C89, C90,C91,C92,C93	100uF	66	1	L3	10mH
31	2	C33,C34	2uF	67	1	C45	100pF
32	2	C32,C22	1uF	68	1	C48	500pF
33	4	D10,D12,D13,D16	1N3600	69	1	IC1	LM360
34	4	D11,D14,D15,D17	1N5235	70	1	R53	680
35	2	J2,J3	BNC	71	1	C52	27
36	2	L1,L2	2.5 uH	72	4	IC2,IC6,U6,U27	74S04
				73	8	IC3,IC4,U13,U14,U19,U20, U21,U24	74121
				74	1	IC5	74S74

## List of Electronic Components (cont.)

Item	Quantity	Reference	Part
75	1	P3	20+1K
76	1	J6	GATE IN
77	1	J7	TRIG OUT
78	1	J8	GATE OUT
79	1	J9	GATE MONITOR
80	1	L5	7 BEADS
81	4	D21, D22, D23, D24	1N4148
82	1	C54	3300
83	1	C55	1500pF
84	1	C53	270pF
85	2	U15, U23	74LS00
86	5	R56, R57, R58, R59, R60	470
87	1	U16	7474
88	2	U17, U18	74LS192
89	2	U22, U25	7404
90	2	C65, C66	47
91	2	R61, R62	10k
92	2	R63, R65	270
93	2	R64, R66	360
94	2	U26, U32	MCL2601
95	3	U28, U29, U31	74S140
96	1	U30	74HCT4046
97	1	R70	5.1K
98	1	R71	50K
99	1	J10	TO
100	1	SW2	BCD SW
101	15	C68, C69, C70, C71, C72, C73, C74, C75, C76, C77, C78, C79, C80, C81, C82	0.1
102	1	C67	470pF
103	1	C62	150pF
104	1	T6	200KVA
105	1	SW3	POWER
106	1	SW5A1	HIGH VOLTAGE
107	2	SW5C1, SW5B1	3P2T
108	1	R72	15K
109	2	D25, D26	LN28RCP
110	4	D27, D28, D29, D30	1N4006

## CHECKLIST

1. Check that all connecting cables are installed. Check color ID's.
2. Turn power ON: main electronic unit, time interval counter, and oscilloscope. Check timer settings and allow 15-30 minutes warmup.
3. Locate wheel fixture, making sure the EMAT will seat flush on the rim of the front face. Check radial position of top plate.
4. Insert EMAT cylinder in wheel fixture. Rotate to first position.
5. Check oscilloscope display for signal strength, and digital gate position and stability.
6. Observe time display for reasonable stability ( $<\pm 10$  ns variation) and record.
7. Rotate transducer  $90^\circ$  and repeat steps 5 and 6.
8. Rotate transducer to original position and repeat steps 5 to 7 about two more times.
9. Average the two sets of data and calculate the birefringence, eq. (1).
10. Subtract the texture birefringence and calculate the stress, eq. (2).

## TROUBLE SHOOTING

Some potential problems with possible solutions include:

- |  |   |
|--|---|
| 1. Poor signal, low amplitude 1st echo   | Check to see that the EMAT is seated properly on the rim face. This will likely mean adjustment of the wheel fixture.   |
| 2. No signal   | The EMAT coil may be shorted or open. Its DC resistance should be about $5 \Omega$ .  |
| 3. Time jitter between successive timer readings ( $>\pm 10$ ns)                       | Adjust the fine control of the digital gate delay.  |
| 4. Time differences between the radial and circumferential signals of about 400-500 ns | The stress level may be very high or the digital gate may be jumping a cycle between the two readings. Check the time-expanded oscilloscope display to be sure the gate TTL signal triggers on the same cycle. Adjust the delay if necessary. |

## FUTURE CONSIDERATIONS

1. It may be possible to stack two sets of EMAT coils, one atop the other, in orthogonal orientations. Connecting first one and then the other coil to the EMAT electronics may permit timing the signals from the two polarizations without physically rotating the transducer.
2. Computer controls are possible to fully automate this procedure:
  - A. Find the center of the acoustic pulse of the first echo and adjust the window of the digital gate.
  - B. Switch between the two coils of #1.
  - C. Use a time interval counter with an IEEE-488 bus to allow direct input.
  - D. Perform all record keeping and calculations.
3. There may be advantages to using ultrasonic waves of other modes. Rayleigh waves would yield specific information on surface conditions. Longitudinal or P-waves can be directed along the surface or through the bulk; in addition, their stress acoustic constant is larger so they would be a more sensitive probe. It may be possible to combine information from the different modes to minimize the texture effects.
4. The BNC coaxial connectors should probably be replaced with a more durable type for long-time field operation.
5. Investigate a more durable wear plate for the contact surface of the EMAT. Experience will indicate whether this is a problem.
6. An enlarged data base on the texture effect will increase the reliability of eliminating this parameter.
7. Experience will dictate modifications to the wheel fixture to increase its flexibility and reliability.

## ACKNOWLEDGMENTS

A considerable number of people have been involved in this work in various ways and at various time.

From the FRA, Clifford Gannett, Claire Orth, and Donald Gray have all provided valuable guidance.

From TTC we received a great deal of help and cooperation in obtaining test wheels. Of course, many tests would have been impossible without their collaboration. Our main contact has been Robert Larson, Jr., who put a great deal of effort into this work. Some of the many others include Britto Rajkumar, Robert Vandeberg, and Robert Florom.

Both before and after his stay as a guest researcher in our laboratory, Professor Hidekazu Fukuoka of Osaka University was a valuable guide to the stress effects on ultrasound, particularly in railroad wheels.

Within our own lab, there have been many helpful ideas and considerable assistance at all stages. We are especially grateful to Dale Fitting, Jon Fowler, Peter Shull (now at the Dept. of Materials Science, Johns Hopkins University), Christopher Fortunko, Daniel Vigliotti, and many others. Tim Waldorf's skills were responsible for producing the wheel fixture. Avinoam Tomer (guest researcher from the Nuclear Research Center Negev, Beer Sheva, Israel) polished and etched the wheel rim cross section.

#### REFERENCES

- [1] "Residual-Stress Measurements Using Shear-Horizontal Waves from Electromagnetic-Acoustic Transducers," R. B. King and C. M. Fortunko, NBSIR 84-3002 (March 1984). (This is a collection of published papers.)
- [2] "Acoustoelasticity and Ultrasonic Measurements of Residual Stresses," Y.-H. Pao, W. Sachse, and H. Fukuoka in Physical Acoustics, Vol. XVII, Academic Press, New York (1984), 61-143.
- [3] "Magneto-Acoustic Stress Responses of Various Rail Metallurgies," D. Utrata and M. Namkung in Review of Progress in Quantitative Nondestructive Evaluation, Vol. 9B, D. O. Thompson and D. E. Chimenti, eds., Plenum Press, New York (1990), 1903-1910.
- [4] DEBRO-30 Stress Meter,\* developed by the Institute of Fundamental Technological Research, Polish Academy of Sciences. Marketed by ELTRONA GmbH, Hamburg, Federal Republic of Germany.
- [5] "The Design and Use of Electromagnetic Acoustic Wave Transducers (EMATs)," B. W. Maxfield and C. M. Fortunko, Materials Evaluation 41, 1399-1408 (1983).
- [6] "Acoustoelastic Measurements of Residual Stresses in the Rim of Railroad Wheels," H. Fukuoka, H. Toda, K. Hirakowa, H. Sakamoto, and Y. Tota in Wave Propagation in Inhomogeneous Media and Ultrasonic Nondestructive Evaluation, Vol. 6, G. C. Johnson, ed., ASME (1984), 185-193.
- [7] B&K model 1822, 175 MHz Universal Counter

---

\* The use of tradenames in no way implies endorsement or approval by NIST and is included only for identification.

- [8] "Ultrasonic Characterization of Residual Stress and Texture in Cast Steel Railroad Wheels," A. V. Clark, H. Fukuoka, D. V. Mitraković, and J. C. Moulder in Review of Progress in Quantitative Nondestructive Evaluation, Vol. 6B, D. O. Thompson and D. E. Chimenti, eds., Plenum Press, New York (1987), 1567-1575.
- [9] "Characterization of Residual Stress and Texture in Cast Steel Railroad Wheels," A. V. Clark, Jr., H. Fukuoka, D. V. Mitraković and J. C. Moulder, Ultrasonics 24, 281-288 (1986).
- [10] "Ultrasonic Characterization of Residual Stress and Flaws in Cast Steel Railroad Wheels," A. V. Clark, R. E. Schramm, H. Fukuoka, and D. V. Mitraković in Proceedings: IEEE 1987 Ultrasonics Symposium, B. R. McAvoy, ed., Institute of Electrical and Electronic Engineers, New York (1988), 1079-1082.
- [11] "Acoustoelastic Measurements Pertaining to the Nondestructive Characterization of Residual Stress in a Heat-Treated Steel Railroad Wheel," A. V. Clark, H. Fukuoka, D. V. Mitraković, and J. C. Moulder, Materials Evaluation 47, 835-841 (1989).
- [12] "Nondestructive Evaluation of Material Properties with EMAT (Formability in Cold Rolled Steel Sheets and Residual Stress in Railroad Wheel)," R. Murayama, K. Fujisawa, H. Fukuoka, M. Hirao, and S. Yonehara in Proceedings: IEEE 1989 Ultrasonics Symposium, B. R. McAvoy, ed., Institute of Electrical and Electronic Engineers, New York (1990), 1159-1162.

# BIBLIOGRAPHIC DATA SHEET

1. PUBLICATION OR REPORT NUMBER	NISTIR 3968
2. PERFORMING ORGANIZATION REPORT NUMBER	
3. PUBLICATION DATE	May 1991

**TITLE AND SUBTITLE**  
 Report No. 23 - Residual Stress Detection in Railroad Wheels: An Ultrasonic System Using EMATs

**AUTHOR(S)**  
 Raymond E. Schramm, Alfred V. Clark, Jr., Dragan V. Mitrakovic, Stephen R. Schaps, and Todd J. McGuire

**PERFORMING ORGANIZATION (IF JOINT OR OTHER THAN NIST, SEE INSTRUCTIONS)**  
 U.S. DEPARTMENT OF COMMERCE  
 NATIONAL INSTITUTE OF STANDARDS AND TECHNOLOGY  
 BOULDER, COLORADO 80303-3328

7. CONTRACT/GRANT NUMBER	DTFR 53-89-X-00018
8. TYPE OF REPORT AND PERIOD COVERED	Final 9/85 - 12/90

**SPONSORING ORGANIZATION NAME AND COMPLETE ADDRESS (STREET, CITY, STATE, ZIP)**  
 U.S. Dept. of Transportation, Federal Railroad Admin.  
 Office of Research and Development, Washington, DC 20590

**10. SUPPLEMENTARY NOTES**

**1. ABSTRACT (A 200-WORD OR LESS FACTUAL SUMMARY OF MOST SIGNIFICANT INFORMATION. IF DOCUMENT INCLUDES A SIGNIFICANT BIBLIOGRAPHY OR LITERATURE SURVEY, MENTION IT HERE.)**

This is report number 23 in a series covering research performed by the National Institute of Standards and Technology for the Federal Railroad Administration. This report covers a project by the Materials Reliability Division (formerly the Fracture and Deformation Division) to develop and build a system to detect and measure residual stress in the rims of railroad wheels.

Acoustic birefringence is the underlying principle of operation. This is a measure of the relative difference in the propagation times of two shear waves polarized in radial and circumferential directions. Measurements employ an EMAT (electromagnetic-acoustic transducer) as an ultrasonic probe. This type of transducer requires little or no surface preparation and no acoustic couplant. The system operates in a pulse-echo mode. A short burst of shear horizontal waves travels through the rim thickness. The rotation of the EMAT determines the orientation of the polarization vector, radial or circumferential. Precise timing of echoes in both directions reveals the degree of birefringence. Changes are due to both stress state and metallurgical texture. Initial tests indicate it may be possible to separate these two.

This report documents the design, construction, and testing of the system. It is also to serve as an operational guide for the equipment being delivered to the FRA.

**2. KEY WORDS (6 TO 12 ENTRIES; ALPHABETICAL ORDER; CAPITALIZE ONLY PROPER NAMES; AND SEPARATE KEY WORDS BY SEMICOLONS)**

birefringence; EMAT; nondestructive testing; railroad wheel; residual stress; ultrasonic

<b>3. AVAILABILITY</b> <input checked="" type="checkbox"/> UNLIMITED <input type="checkbox"/> FOR OFFICIAL DISTRIBUTION. DO NOT RELEASE TO NATIONAL TECHNICAL INFORMATION SERVICE (NTIS). <input type="checkbox"/> ORDER FROM SUPERINTENDENT OF DOCUMENTS, U.S. GOVERNMENT PRINTING OFFICE, WASHINGTON, DC 20402. <input checked="" type="checkbox"/> ORDER FROM NATIONAL TECHNICAL INFORMATION SERVICE (NTIS), SPRINGFIELD, VA 22161.	<b>14. NUMBER OF PRINTED PAGES</b>  48
	<b>15. PRICE</b>

ELECTRONIC FORM





NISTIR 3968  
Jun 13, 2016

